Natural ventilation assessment in typical open an semi-open urban environments under various wind directions

Article

Accepted Version

Natural ventilation assessment in typical open and semi-open urban environments under various wind directions

Jian Hang, Zhiwen Luo, Mats Sandberg, Jian Gong

PII: S0360-1323(13)00260-6

DOI: 10.1016/j.buildenv.2013.09.002

Reference: BAE 3509

To appear in: *Building and Environment*

Received Date: 20 June 2013

Revised Date: 2 September 2013

Accepted Date: 5 September 2013

>Semi-open street roofs protect pedestrians from strong sunshine and heavy rains. >But they may affect airflows and ventilation in urban canopy layers (UCL).> Age of air & flow rates are analyzed under wind directions of 0^{o},15^{o},30^{o}, 45^{o}.>Walls fully or partly covering street roofs at z=H get the worst UCL ventilation.> Semi-open street roofs at z=1.2H,1.1H get good ventilation and are realistic designs.

To be resubmitted to Building and Environment, September 2013

Natural ventilation assessment in typical open and semi-open urban environments under various wind directions

Jian Hang[a*], Zhiwen Luo[b], Mats Sandberg[c], Jian Gong[d]

[a]Department of Atmospheric Sciences, School of Environmental Science and Engineering, Sun Yat-Sen University, Guangzhou, Guangdong, P. R. China
[b] School of Construction Management and Engineering, University of Reading, Reading, UK
[c] Laboratory of Ventilation and Air Quality, University of Gävle, SE-80176 Gävle, Sweden
[d]School of Civil Engineering and Architecture, Nanchang Hangkong University, Nanchang, Jiangxi, 330063, P. R. China

*Corresponding author. Jian Hang
Tel: +86-20-84110375; fax: +86-20-84110375
E-mail address: hangj3@mail.sysu.edu.cn

Abstract

Semi-open street roofs protect pedestrians from intense sunshine and rains. Their effects on natural ventilation of urban canopy layers (UCL) are less understood. This paper investigates two idealized urban models consisting of 4(2×2) or 16(4×4) buildings under a neutral atmospheric condition with parallel (0^o) or non-parallel (15^o,30^o,45^o) approaching wind. The aspect ratio (building height (*H*) / street width (*W*)) is 1 and building width is $B=3H$. Computational fluid dynamic (CFD) simulations were first validated by experimental data, confirming that standard k-ε model predicted airflow velocity better than RNG k-ε model, realizable k–ε model and Reynolds stress model. Three ventilation indices were numerically analyzed for ventilation assessment, including flow rates across street roofs and openings to show the mechanisms of air exchange, age of air to display how long external air reaches a place after entering UCL, and purging flow rate to quantify the net UCL ventilation capacity induced by mean flows and turbulence.

Five semi-open roof types are studied: Walls being hung above street roofs (coverage ratio λ_a=100%) at z=1.5H, 1.2H, 1.1H ('Hung1.5H', 'Hung1.2H', 'Hung1.1H' types); Walls partly covering street roofs (λ_a=80%) at z=H ('Partly-covered' type); Walls fully covering street roofs (λ_a=100%) at z=H ('Fully-covered' type).They basically obtain worse UCL ventilation than open street roof type due to the decreased roof ventilation. 'Hung1.1H', 'Hung1.2H', 'Hung1.5H' types are better designs than 'Fully-covered' and 'Partly-covered' types. Greater urban size contains larger UCL volume and requires longer time to ventilate. The methodologies and ventilation indices are confirmed effective to quantify UCL ventilation.

Key words: Semi-open street roof; natural ventilation; age of air; purging flow rate; CFD simulations; wind tunnel experiment

1. Introduction

Wind from rural areas provides cleaner rural air into urban canopy layers (UCL) to help pollutant and heat dilution. Good UCL ventilation has been known as one of the possible mitigation solutions to improve urban air environments[1-11], meanwhile ameliorate indoor air quality through building ventilation systems.

Complemented by wind tunnel/field experiments, computational fluid dynamics (CFD) simulations have been widely used to predict turbulent airflow, mass transports and energy budgets within, close to and above different UCLs [2,4-11, 17-26, 28-37], ranging from street canyons, street intersections, cavities and courtyards, up to structured building arrays and realistic urban areas. Good reviews on this topic can be found in the literatures [12-15]. For two-dimensional (2D) street canyons [1, 15-19], street aspect ratio (building height/street width, H/W) is the first key parameter to affect the flow regimes and pollutant dispersion. For three-dimensional (3D) urban canopy layers, total street length or urban size [8,11,30], building packing density and frontal area density [8,10,20-23], ambient wind directions [23-24, 32, 37], building layouts and height variations [8, 21-23, 25-26] etc, are significant parameters and have been widely investigated.

In addition to the widely studied urban models with open street roofs, semi-open street roof is one of popular urban design elements existing in the realistic urban areas to protect pedestrians from strong sunshine and reduce the inconveniences in rainy or snowy days. Such semi-open street roofs have been reported and investigated by experiments and CFD simulations in the literatures [5-7], including a large naturally ventilated semi-open market building [5], a semi-open shopping mall being located in Lisbon, Portugal [6], enclosed-arcade (or semi-open) markets of Korea with eleven arcade-type designs (or semi-open street roof) [7]. Although the requirements of design are different according to various climate conditions, sufficient natural UCL ventilation has been considered as an important environment design factor for more healthy semi-open outdoor environments [5-7]. Fig. 1 shows two other kinds of semi-open street roof designs in the suburb of Guangzhou China, which are located in a subtropical region annually characterized by intense solar radiation and precipitation. Fig. 1a shows walls being hung above street roofs of a food court, and Fig. 1b displays walls partially covering street roofs of a retail center. Each shop or restaurant has its own enclosed space with air conditioners inside for cooling in summer (April to September) and with doors connected to the semi-open streets. These semi-open outdoor environments are naturally ventilated to reduce energy consumption. Such semi-open street roof designs are used to provide convenience for pedestrians, but they possibly deteriorate UCL ventilation performance. This paper aims to quantitatively evaluate these effects. Although thermal buoyancy force induced by temperature difference and atmospheric stability also influence urban airflows and UCL ventilation [19, 28-29], this paper takes the first step to consider a neutral atmospheric condition assuming that the ambient wind velocity is sufficiently large and thermal effects are negligible.

In building ventilation, as reviewed by Chen [27], indoor ventilation indices have been widely used to evaluate how external air enters a room and ventilates it. In recent years, researchers have started to apply similar concepts to estimate UCL ventilation [2,4-11, 24, 28-32, 37], including ventilation flow rate and air change rate per hour (ACH) [4, 6-7, 28-30], pollutant exchange rate [31], pollutant retention time and purging flow rate [2,8, 24], age of air and air exchange efficiency [32], city breathability [10-11] etc. This paper emphasizes the quantitative analysis of UCL ventilation induced by rural wind assuming that rural air is relatively clean. Flow rates across street openings and street roofs are first analyzed to quantify the mechanisms of air exchange [37], moreover the local mean age of air [32] is used to quantify how long the external air can reach a place after it enters the UCL. Finally, the UCL purging flow rate [2, 8] is also applied to estimate the net UCL ventilation capacity induced by both mean flows and turbulent diffusions.

Tracer gas techniques [27, 44] are usually used to measure indoor ventilation indices. However for both open or semi-open outdoor spaces, ventilation indices such as age of air and purging flow rate are difficult to be measured by tracer gas techniques, since outdoor environment is not an enclosed space with more complicated openings than indoor, moreover perfect mixing and uniform pollutant generation rate in UCLs are difficult to experimentally control. Thus the literatures [5-11, 24, 28-32] usually use experimental data to validate the reliability of CFD methods in predicting concentration and airflow field, then analyze outdoor ventilation indices by using CFD simulations. This paper also utilizes similar methodologies.

2. Methodologies

2.1 Turbulence modeling in CFD simulations

Large eddy simulation (LES) models are known to perform better in predicting turbulent flows than the Reynolds-Averaged Navier-Stokes (RANS) approaches, but the applicability of LES models is more problematic due to its much longer computational time required than RANS approaches and some issues regarding the implementation of wall and inlet boundary conditions [33-34]. Considering that RANS turbulence models are more time-saving and provide reasonable results for mean flows and the spatial average flow properties [33], this paper adopted RANS turbulence models for evaluating UCL ventilation.

UCL ventilation relies on both mean flows and turbulence within the UCL [8, 37]. According to the literatures [35-36], the modified k–ε models, for example RNG k–ε model, are able to correct the drawback of the standard k–ε model that severely over-predicts turbulent kinetic energy in separated flows around front corners of buildings, however, they fail to predict the sizes of reattachment lengths behind buildings and under-predict the velocity in weak wind regions. It is desirable to compare different RANS turbulence models in predicting urban airflows and UCL ventilation to provide a sensitivity study, including standard k–ε model, RNG k–ε model, realizable k–ε model and Reynolds stress model (RSM).

2.2 Experimental and CFD set-ups in the validation case

This paper aims to study UCL ventilation in low-rise idealized and typical urban models consisting of two-storey buildings (about 7m tall). Wind tunnel data was first used to evaluate the reliability of CFD methodologies. As shown in Fig. 2a, Hang et al. [37] performed some wind tunnel experiments to investigate the flow in a small-scale urban model with four square building blocks (building height H=0.069m, building width B=3H) and two crossing streets (street width W=H, urban size L =7 H). The approaching wind was parallel to the main street and perpendicular to the secondary streets. The scale ratio between small-scale and full-scale models is 1:100. Thus in full-scale real conditions H=$W\approx$7m, B=3$H\approx$21m, $L\approx$49m. In small-scale models the height of 1.5 mm (0.22H) corresponds to the face level (1.5 m) in full-scale conditions.

The measurements were performed in the closed-circuit type wind tunnel at the Laboratory of Ventilation and Air Quality, University of Gävle, Sweden, with the working section of 11m long, 3m wide,1.5m tall. Thus the blockage ratio is about 0.6%, which represents the percentage of the small-scale urban model obstructing the test section area (3m×1.5m) of the wind tunnel. The stream-wise, lateral and vertical directions are represented by x, y, z. Hotwire anemometer was used to measure vertical profiles of velocity ($U_m(z)$) and turbulence intensity ($I(z)$) in the upstream free flow of wind tunnel (see Fig. 2b), horizontal profiles of velocity $\bar{u}(x)$ and turbulence intensity $I(x)$ along the main street centerline (see Fig. 3b) at z=0.11H (7.5mm). The sampling frequency was 100 Hz. The measurement time was 30s for each point. It is worth mentioning that, the hotwire is only sensitive to velocity components perpendicular to it (i.e. the vertical velocity $\bar{w}$ and the stream-wise velocity $\bar{u}$). So data measured by the hotwire were actually $\sqrt{\bar{u}^2+\bar{w}^2}$. Here the hotwire was only located where the span-wise (y) velocity $\bar{v}$ was zero, including in the upstream free flow and along the main street centerline, so the measured data were actually the velocity magnitude (U=$\sqrt{\bar{u}^2+\bar{v}^2+\bar{w}^2}$).

Because there were no roughness elements in wind tunnel experiments, a thin neutral atmospheric boundary layer (ABL) and a sharp vertical profile of velocity was produced in the upstream free flow (see Fig. 2b). We only used the measured profiles ($U_m(z)$ and $I(z)$) in Fig. 2b to provide boundary conditions at domain inlet in the CFD validation case. At domain inlet, turbulent kinetic energy is defined as $k(z)=1.5(I\ U_m)^2$ and its dissipation rate is $\varepsilon(z)=C_\mu^{3/4}k^{3/2}/l$, where C_μ=0.09 and l is the turbulent characteristic length scale. Note that, the maximum velocity in the upstream free flow of wind tunnel experiments was 13.33 m/s, however in cases for ventilation analysis, we used a realistic approaching wind (see Eq. (1a)) with a spatial mean velocity of about 3.2 m/s, so in the validation case we actually utilized a smaller fitting velocity profile (maximum velocity is 3.24 m/s, see Fig. 2b) with the same thickness of ABL as that in wind tunnel and the similar spatial mean velocity (about 3.2m/s) as that in Eq. (1a). According to Snyder [39], Reynolds-number independence can be satisfied if the Reynolds number is greater than 4000, i.e. the main structure of turbulence can be almost entirely responsible for the bulk transport of momentum and heat or mass transfer. If the velocity $z=H=0.069$m in the upstream free flow (see Fig. 2b) is defined as the reference velocity $U_{\mathrm{ref}} \approx 2.94$m/s, the reference Reynolds number ($Re_H = \rho U_{\mathrm{ref}} H/\mu \approx 13887$) is much larger than 4000, Thus the technique of using a smaller inflow velocity (i.e. 3.24m/s) can ensure Reynolds number independence.

The CFD code FLUENT 6.3 [38] was used to solve the steady-state isothermal turbulent flows. For CFD simulations, we used the same small-scale urban geometries (H=0.069m) as those in wind tunnel experiments. Only half computational domain was used to reduce the calculation time. Fig. 3a displays the computational domain and boundary conditions in the CFD validation case. The computational domain is 14.5H wide (1 m) in the lateral (y) direction and 11H tall (0.75 m) in the vertical (z) direction. Thus the blockage ratio is about 1.9% (less than 3%) satisfying the requirement of the literature [40]. No-slip wall boundary condition was utilized at wall surfaces, and zero normal gradient boundary condition was used at domain outlet, domain roof, domain lateral boundary, domain symmetry boundary.

Fig. 3b displays the grid arrangements in x-y plane of the validation case. Finer grids are produced within the UCL and near wall surfaces, building corners, street openings. The grid size near the ground is 0.036H(dz=2.5mm). There are 6 cells vertically from z=0 to the pedestrian height (z=20mm=0.29H).The grid size near building roofs at z=H is 0.022H (dz=1.5mm). The horizontal grid size (dx and dy) near building surfaces varies from 0.022H to 0.043H. The maximum expansion ratio from building surfaces to the surrounding is 1.15 and the total number of hexahedral cells is about 0.82 million.

In the CFD validation case, all CFD set-ups including computational domain size, boundary conditions and grid arrangements fulfilled the major CFD guidelines recommended by Tominaga et al. [40].

2.3 CFD set-ups for flow modelling

After the CFD validation case, more urban configurations with or without semi-open street roofs and various ambient wind directions were investigated. To better illustrate idealized urban models, all test cases were defined as Case [number of rows-number of columns, wind direction, roof type]. 'Open' roof type denotes open street roofs; As shown in Fig. 4a-4c, four wind directions of 0^o, 15^o, 30^o, 45^o were included. So the name of validation case is Case [2-2, 0, Open] with four buildings (2 rows, 2 columns), a parallel approaching wind (0^o) and open street roof ('Open' roof type). As displayed in Fig. 4c, a bigger urban model with 16 buildings (4 columns, 4 rows, urban size L=15H≈105m in full scale) was also investigated in CFD simulations. Besides the 'Open' roof type, Fig. 5 shows the other five types studied in CFD simulations. 'Fully-covered' roof type (see Fig. 5a) means walls entirely covering street roofs with a coverage ratio(λ_a) of 100% at z=H, and 'Partly-covered' roof type (see Fig. 5b) represents street roofs being partly covered (λ_a=80%) by walls at z=H. Roof types of 'Hung1.5H', 'Hung1.2H' and 'Hung1.1H' (see Fig. 5c) represent walls being hung above street roofs (λ_a=100%) at z=1.5H, 1.2H and 1.1H, respectively. As summarized in Table 1, total 48 test cases were numerically investigated.

For test cases with a parallel approaching wind (0^o), the computational domain and boundary conditions were similar as the CFD validation case. A power-law velocity profile was applied at domain inlet with a power-law exponent of 0.16(see Eq. (1a)). As reported by Lien and Yee [41], it represents a neutral atmospheric boundary layer (ABL) with a depth of 1.8 m created in the wind tunnel by using spires and floor roughness with a roughness length of approximately z_0=0.001 m. In full-scale real conditions, it corresponds to a neutrally-stratified ABL with a surface roughness of z_0=0.1m [42] (i.e. a neutral ABL above open rural area with a regular cover of low crop and occasional large obstacles [43]) The spatial mean velocity at domain inlet calculated from Eq. (1a) approximately equals to that calculated from the inflow velocity profile of the CFD validation case (see Fig. 2b).The inlet profiles of turbulent kinetic energy and its dissipation rate were calculated by Eq. (1b)-(1c)) [30,41].

$$\bar{u}(z) = U_0(z) = U_H(z/H)^{0.16}, \bar{v}(z) = \bar{w}(z) = 0 \tag{1a}$$

$$k_0(z) = u_*^2 / \sqrt{C_\mu} \tag{1b}$$

$$\varepsilon_0(z) = C_\mu^{3/4} k_0(z)^{3/2} / (\kappa_v z) \tag{1c}$$

where the friction velocity u_*=0.24 ms^{-1}, $\kappa_v = 0.41$ is von Karman's constant, U_H=2.66ms^{-1} is the reference velocity at z=H=0.069m of domain inlet.

For test cases with a non-parallel approaching wind (15^{o}, 30^{o} , 45^{o}), there are two domain inlets and two domain outlets(see Fig. 4a). At domain inlets, the power-law velocity profiles (stream-wise velocity $\overline{u}$ =U_0(z)cosθ, span-wise velocity $\overline{v}$ =U_0(z)sinθ and vertical velocity $\overline{w}(z) = 0$) and profiles of turbulent quantities in Eq. (1b)-(1c) were used to provide boundary conditions. Zero normal gradient conditions were still used at two domain outlets and domain roof.

Fig. 6a and 6b show two examples of the grid arrangements in test cases with four (2×2) buildings and semi-open street roofs. Note that, the thickness of hung walls to produce semi-open street roofs was zero in CFD models. The grid arrangements were similar with those in the CFD validation case except three points: The first is that the grids near semi-open street roofs (i.e. at z=1.1H, 1.2H, 1.5H) are also fine with a grid size of dz=0.014H=1mm (see Fig. 6b); The second is that for test cases with 16 buildings the maximum expansion ratio of grid size from wall surfaces to the surrounding is 1.2 which is less than 1.3 and satisfies the CFD guideline [40];The third is that the grid number in cases with ' Partly-covered' roof type (see Fig. 6a) is a little more than the other roof types, because fine grids with grid size of dy=0.029H were also generated near lateral boundaries of partly-covered street roofs. The maximum grid number is about 3.5 million in Case [4-4,45, Partly-covered].

All transport equations were discretized by the second order upwind scheme to increase the accuracy and reduce numerical diffusion. The SIMPLE scheme was used for the pressure and velocity coupling. CFD simulations were run until all residuals became constant. Overall, residual for the continuity equation was below 10^{-4}, residuals for the velocity components and k were below 10^{-7}, residuals for pollutant concentration and ε were below 0.5×10^{-5} and 0.5×10^{-4} respectively.

2.4 Ventilation assessment indices

2.4.1 Age of air

The local mean age of air (τ_p) was originally defined in indoor ventilation and can be measured by tracer gas techniques [44]. The local age of air in UCLs represents the mean time required for the external young air to reach a point since it enters UCLs. If the age of air in rural areas is zero, the greater age of air in UCLs represents a greater probability to be polluted. The

UCL age of air depicts how rural air is supplied and distributed within UCLs. Hang et al. [32] first introduced the homogeneous emission method [44] to numerically predict age of air in UCLs.

The governing equations of time-averaged pollutant concentration ($\bar{c}$, kg/m^3) and the age of air (τ_p, s) are displayed as below:

$$\bar{u}_j \frac{\partial \tau_p}{\partial x_j} - \frac{\partial}{\partial x_k}\left(K_c \frac{\partial \tau_p}{\partial x_k}\right) = 1 \qquad (2)$$

$$\bar{u}_j \frac{\partial \bar{c}}{\partial x_j} - \frac{\partial}{\partial x_j}\left(K_c \frac{\partial \bar{c}}{\partial x_j}\right) = S_c \qquad (3)$$

where $\bar{u}_j$ is the velocity components ($\bar{u}, \bar{v}, \bar{w}$) in the stream-wise ($x$), span-wise ($y$) and vertical ($z$) directions, $K_c = \nu_t / S_{ct}$ is the turbulent eddy diffusivity of pollutants, ν_t is the kinematic eddy viscosity, S_{ct} is the turbulent Schimdt number (S_{ct}=0.7) [8, 10, 20, 45]. S_c is the pollutant source term (kgm^{-3}s^{-1}).

In the homogeneous emission method[44], a relation between these two variables was mathematically derived. If a homogenous pollutant release rate (S_c, kgm^{-3}s^{-1}) is defined in the entire UCL, the age of air (τ_p, s) can be calculated:

$$\tau_p = \bar{c} / S_c \qquad (4)$$

Eq. (4) illustrates a relationship that, with a uniform pollutant source in the entire UCL, higher pollutant concentration at a point represents that it takes the external clean air a longer time to arrive.

Fig.6c shows an example of defining uniform pollutant source in the entire UCL. In this paper, the pollutant emission rate was small (S_c=10^{-7}kg m^{-3}s^{-1}) to ensure the source release producing little disturbance to the flow field. The inflow concentration at domain inlet was defined zero, and the zero normal flux condition was used at wall surfaces. At all other boundaries zero normal gradient condition was utilized.

Because the age of air in small-scale urban models is small (scale ratio 1:100), the age of air was normalized in Eq. (5a). To compare the age of air in the entire UCLs, this paper also analyzed the normalized spatial mean age of air ($<\tau_p^*>$) in Eq. (5b)

$$\tau_p^* = \tau_p \times 100 \qquad (5a)$$

$$<\tau_p^*> = \int_{Vol} \tau_p^* dxdydz / Vol \quad (5b)$$

where *Vol* is the entire UCL volume.

2.4.2 Ventilation flow rates and UCL purging flow rates

Both mean flows and turbulent diffusions are significant factors for UCL ventilation [37] and pollutant removal [8]. The purging flow rate represents the net flow rate induced by both mean flows and turbulent diffusions for a volume to be purged out by wind through it. It has been used to quantify the ventilation in UCLs [2] and at the pedestrian levels [8].

This paper mainly emphasizes the purging flow rate for the entire UCL. If a passive contaminant source is generated within the entire UCL (see Fig. 6c) with a uniform emission rate (here $S_c=10^{-7}$ $kgm^{-3}s^{-1}$), the UCL purging flow rate (*PFR*, m^3/s) is calculated in Eq. (6).

$$PFR = \frac{S_c \times Vol}{<\bar{c}>} = \frac{S_c \times Vol}{\int_{Vol} \bar{c} dxdydz / Vol} \quad (6)$$

Here $<\bar{c}>$ is the spatially-averaged concentration in the entire UCL volume (Vol) . It is worth mentioning that *PFR* is independent of pollutant sources, and illustrates the net UCL ventilation capacity due to both mean flows and turbulent diffusion.

Because *PFR* is small for small-scale urban models (scale ratio 1:100), *PFR* is normalized by the reference flow rate (Q_∞).

$$PFR^* = \frac{S_c \times Vol}{<\bar{c}> Q_\infty} = \frac{PFR}{Q_\infty} \quad (7)$$

$$Q_\infty = H \times \int_0^H U_0(z) dz \quad (8)$$

where $Q_\infty = 0.01093$ m^3/s is the flow rate far upstream through the same area with a windward street opening (area $A = H \times H$), $U_0(z)$ is defined in Eq. (1a).

Fig. 4b-4c show the definition of street openings in test cases with 4 (2×2) and 16 (4×4) buildings. To quantify the ventilation pattern, all flow rates entering and leaving UCL volumes were normalized by the reference flow rate (Q_∞), including Q^* due to mean flows (see Eq. (9)) and $Q^*_{roof}(turb)$ due to turbulence fluctuations across street roofs [37] (see Eq. (10)):

$$Q^* = \int_A \vec{V} \bullet \vec{n} dA / Q_\infty \qquad (9)$$

$$Q*_{roof}\ (turb) = \pm \int 0.5\sigma_w dA / Q_\infty \qquad (10)$$

where in Eq.(9), $\vec{V}$ is velocity vector, $\vec{n}$ is the normal direction of street openings or street roofs, A is surface area; In Eq.(10), $\sigma_w = \sqrt{\overline{w'w'}} = \sqrt{2k/3}$ is the fluctuation velocity on street roofs based on the approximation of isotropic turbulence (k is the turbulent kinetic energy).

Due to the flow balance by mean flows, the total flow rate leaving UCL (Q_{out}) through UCL boundaries equals to that entering UCL (Q_{in}). They are named as the total flow rates by mean flows Q_T and are normalized by the reference flow rate Q_∞.

$$Q_T* = Q_{in}* = Q_{out}* \qquad (11)$$

By applying the above concepts, this paper quantifies the effects of semi-open street roofs and various wind directions on the age distribution, the ventilation pattern and the entire UCL ventilation capacity.

3. Results and discussions

3.1 Evaluation and validation of CFD results

Fig. 7 shows the validation of CFD results by using the measured horizontal profiles of velocity and turbulent intensity along street centerline at z=0.11H in Case [2-2.0, Open]. x/H=0 denotes the location of windward street opening (at O1). The velocity was normalized by the inflow velocity at domain inlet at the same height (z=0.11H). In comparison to wind tunnel data, the standard k-ε model and realizable k-ε model predicted the velocity profile better than RNG k-ε model and RSM model. More importantly the standard k-ε model performed the best in predicting airflow velocity in the downstream region of the main street. This finding agrees with the literature [35-36] that non-standard k-ε models perform better in predicting separate flows but do worse in predicting airflow velocity in weak wind regions. All RANS turbulence models can only predict the shape of turbulence intensity profile, thus $Q*_{roof}$(turb) calculated by CFD simulations were only used to provide a reference study and the relative values of $Q*_{roof}$(turb) among different test cases were emphasized. Since the better prediction of mean flows within

UCL and along the streets is more important, this paper hereby regards the standard k-ε model as the default turbulence model in the following CFD simulations.

For the validation case (medium grid, 0.8 million), a finer grid arrangement with the minimum grid size of 0.014*H* and grid number of 1.3 million was used to perform a grid independence study. As displayed in Fig. 7c, numerical results were not sensitive to the grid refinement, indicating present grid arrangements in Fig. 3b were sufficiently fine.

3.2 Ventilation assessment in cases with four buildings

In this subsection, the effects of semi-open street roofs and various wind directions in test cases with four buildings and two crossing streets (i.e. Case [2-2,wind direction, roof type], see Table 1) were investigated.

3.2.1 Effect of semi-open street roofs in four example test cases

Fig. 8a displays three-dimensional (3D) streamline in four test cases (only half domain, 0^o), i.e. Case [2-2, 0, Open], Case [2-2, 0, Hung1.2H], Case [2-2, 0,Partly-covered], Case [2-2, 0,Fully-covered]. Channel flows are found in the main streets parallel to the approaching wind and 3D helical flows exist in the secondary streets. These channel and helical flows produce air exchange and turbulent diffusion through street openings and street roofs. Different semi-open street roofs may produce various flow pattern and ventilation capacity but this effect cannot be clearly displayed by only 3D streamlines in Fig. 8a. To quantify this effect, Fig. 8b shows the normalized age of air ($\tau_p{*}=\tau_p\times 100$) in z=0.22*H* (i.e. 1.5m in full scale) and normalized flow rates (Q*) in these four test cases. Positive values denote air entering UCLs and negative ones represent air leaving UCLs. $\tau_p{*}$ along the main street (Street 1 and Street 3) is relatively small (i.e. air is relatively young) because Q* through O1 and O3 are always large (Q*(O1)=1.048 to 0.848; Q*(O3)=-0.551 to -0.813). In the secondary streets (Street 2 and Street 4), Q* through O2 (O4) are small (only 0.086 to -0.019). Thus the roof ventilations are more significant to the secondary streets. For example, in Case [2-2, 0, Open], $\tau_p{*}$ in Street 2 (or Street 4) is similar with that in Street 3 because the flow rates across street roofs are comparable to those across O1 and O3, including the upward and downward flow rates due to mean flows (Q^*_{roof}(out)=-0.825 and Q^*_{roof}(in)=0.148), and the effective flow rate induced by turbulence fluctuations

(Q^*_{roof}(turb)= 1.211). For types of 'Hung1.2H' and 'Partly-covered', roof ventilation capacity significantly decreases, including Q^*_{roof}(out)=-0.825 to -0.424 and -0.306, Q^*_{roof}(in)=0.148 to 0.116 and 0.008,Q^*_{roof}(turb)=1.211 to 1.059 and 0.258. Moreover Q^* across O1 decreases a little (1.048 to 0.999 and 0.950) due to the displacement by semi-open street roofs, and Q^* across O3 increases a little (-0.551 to -0.684 and -0.685). These results show that semi-open street roofs not only pose additional flow resistances and therefore reduce the ventilation by vertical mean flows and turbulence across street roofs, but also influence the inflow rates and redistribution of airflows along the streets within UCL, especially driving more air across Street 3 (O3). Thus in contrast to Case [2-2, 0, Open], models with semi-open street roofs obtain much greater τ_p* and older air in the secondary streets due to the weakened roof ventilation. An extreme example is 'Fully-covered' type, in which the flow rates across street roofs are zero, and τ_p* in the secondary street (125 to 225) is much greater than that in the main street (0-45). The UCL spatial mean age of air $<\tau_p*>$ with 'Open' and 'Hung1.2H' types are 24.3 and 37.7, which is much smaller than $<\tau_p*>$ with 'Partly-covered' and 'Fully-covered' types (54.9 and 90.4), confirming that the 'Hung1.2H' type provide better overall UCL ventilation than 'Partly-covered' and 'Fully-covered' types.

3.2.2 Effect of ambient wind directions in four example test cases

Fig. 9 displays 3D streamline, τ_p* and Q^* in Case [2-2, 0, Hung1.5H], Case [2-2, 15, Hung1.5H], Case [2-2, 30, Hung1.5H] and Case [2-2, 45, Hung1.5H]. The flow patterns are obviously different and flow rates are redistributed. With a parallel approaching wind, air enters UCL through O1, O2 and O4, then leaves through O3. Moreover 3D helical flows mainly exist in Street 2 and Street 4 where air is relatively old. With non-parallel approaching wind, air enters UCLs across O1 and O2, then leaves through O3 and O4; Recirculation flows exist in all four streets and τ_p* is relatively large in the downstream streets (Street 3 and Street 4) and in recirculation regions. If wind directions change from 0^o to 15^o, 30^o, 45^o, both roof ventilation and overall UCL ventilation are improved including Q^*_{roof}(out) varies from -0.547 (0^o) to -0.939(15^o), -0.919 (30^o) and -0.730 (45^o), Q^*_{roof}(in) changes from 0.106 (0^o) to 0.586(15^o), 1.092 (30^o) and 1.041(45^o)), and $<\tau_p*>$ decreases from 29.6 (0^o) to 22.6 (15^o), 18.9 (30^o) and 18.5 (45^o). These results confirm that 30^o and 45^o produce better UCL ventilation than 0^o and 15^o.

As discussed and reported by the literature [2, 8-11, 18-20, 24, 31-32, 45],turbulent Schimdt numbers (S_{ct}) may influence numerical results of pollutant dispersion. As displayed in Table 2, the effects of different S_{ct} and turbulence models are studied in Case [2-2, 0, Open] to quantify the sensitivity of turbulence models and S_{ct} on UCL ventilation: S_{ct} =1.0, 0.7 and 0.4 are used in standard k-ε model, S_{ct}=0.7 in RNG k-ε model, and S_{ct} =0.7 in Realizable k-ε model. With the same standard k-ε model and S_{ct} of 1.0, 0.7 or 0.4, $<\tau_p^*>$ in the entire UCL are 26.4, 24.3 and 21.2, respectively, showing that smaller S_{ct} may enhance pollutant dispersion by turbulent diffusion and slightly reduce the age of air. With the same S_{ct} of 0.7, realizable k-ε model and RNG k-ε model obtain different flow rates through O3 and street roofs which result in a little greater $<\tau_p^*>$ (27.2 and 28.2) than that by standard k-ε model (24.3). Especially Q^* across O3 predicted by RNG k-ε model is much smaller than those by the other two, which can be explained by the fact that RNG k-ε model significantly over-predicts Q^*_{roof}(out) (-1.127) than the other two (-0.825 and -0.844). To be consistent, standard k-ε model with S_{ct} of 0.7 was selected as the default settings in CFD simulations.

3.2.2 Overall ventilation assessment in cases with four (2×2) buildings

To quantify the effect of semi-open street roofs on UCL ventilation flow rates, Fig. 10 shows Q^* through O1-O4 and Q^*_{roof}(out), Q^*_{roof}(in), Q^*_{roof}(turb) in all test cases with 4 buildings and wind directions of 0^{o} to 45^{o}. Roof types change from 'Open', 'Hung1.5H', 'Hung1.2H', 'Hung1.1H', to 'Partly-covered' and 'Fully-covered' (reading figure from left to right). Roof ventilations for 'Fully-covered' type are all zero. For wind directions of 0^{o} and 15^{o} (see Fig.10a-10b), roof type variations result in a slightly decreasing flow rates across O1 and an increasing flow rates across O3. More importantly, the flow rates across street roofs are all significantly weakened, including Q^*_{roof}(out) from -0.825 (0^{o}) and -1.156(15^{o}) to 0, Q^*_{roof}(in) from 0.148 (0^{o}) and 0.619 (15^{o}) to 0, and Q^*_{roof}(turb) from 1.211(0^{o}) and 1.315 (15^{o}) to 0. Moreover, Q^* across O2 and O4 are relatively small for wind direction of 0^{o} (see Fig. 10a), but they become considerably large for wind direction of 15^{o} (see Fig. 10b). For wind directions of 30^{o} and 45^{o} (see Fig.10c-10d), similar findings exist due to such roof type variations that all roof ventilation indices decrease quickly and Q^* across street openings decrease a little.

To quantify the reduction of UCL ventilation as roof types varying from 'Open' type to 'Fully-covered' type, the normalized ventilation ratio (*NVR*) is defined as the value of ventilation indices in a case divided by those with 'open street roofs' and the same wind direction. Thus for cases with open street roofs, *NVR*=1, and Q^* across street roofs for 'Fully-covered' roof type are all zero (*NVR*=0). Fig. 11displays Q^*_{roof} (in) and Q^*_{roof} (out), Q^*_{roof} (turb), total normalized flow rates by mean flows (Q_T^*), normalized UCL purging flow rate (*PFR**), $<\tau_p*>$ in the entire UCL, and their *NVR* values for all 24 cases with 4 buildings. With the same roof type, wind direction of 30^o and 45^o obtain greater Q^*_{roof} (in) and Q^*_{roof} (turb), larger Q_T^* and *PFR**, smaller $<\tau_p*>$, showing that 30^o and 45^o produce better UCL ventilation than 0^o and 15^o. In addition, Fig.11a-11b also confirm that, all roof ventilation indices decrease as roof type varies from 'Open' to 'Partly-covered' , and *NVR* for 'Partly-covered' type are as small as 5.6% to 34% for Q^*_{roof} (in), 18.0%-37.1% for Q^*_{roof} (out), and 21.3%-22.6% for Q^*_{roof} (turb) respectively. Fig. 11c-11d displays that overall UCL ventilation basically decreases from 'Open' type to 'Fully-covered' type, indicated by the fact as below: the *NVR* of Q_T^* are 87%-99% for 'Hung1.5H' type, 81%-92% for 'Hung1.2H' type, 67%-78% for 'Hung1.1H' type, 57%-72% for 'Partly-covered' type and 41%-62% for 'Fully-covered' type; the *NVR* of *PFR** are from 82%-110%, 64%-110%, 52%-104% to 44%-87% and 27%-64%, and the *NVR* of $<\tau_p*>$ are from 90%-122%, 91%-155%, 96%-190% to 115%-226% and 156-373%. Overall, Fig. 11d-11e confirm that roof types of 'Hung1.5H', 'Hung1.2H' and 'Hung1.1H' may produce relatively considerable UCL ventilation in contrast to 'Open' type (i.e. *NVR* are 52%-110% for *PFR** and 91%-190%for $<\tau_p*>$). Considering 'Hung1.1H' and 'Hung1.2H' types are more realistic, they are proposed as better semi-open street roof configurations. Meanwhile, Fig. 11d-11e also verify that, if roof types change from 'Open'' to 'Fully-covered', overall UCL ventilation with 0^o wind direction may decrease much more significantly (*NVR* are 100% to 27% for *PFR**, and 100% to 372% for $<\tau_p*>$) than the other wind directions, because the secondary streets with 0^o wind direction and semi-open street roofs tend to be poorly ventilated.

3.3 Ventilation assessment in test cases with sixteen buildings

What happen if urban size enlarges? To quantify this effect, test cases with 16 buildings are investigated, as summarized in Table 1. Fig. 12 displays normalized age of air in four test cases, i.e. Case [4-4, 0, Hung1.2H], Case [4-4, 15, Hung1.2H], Case [4-4, 30, Hung1.2H], Case [4-4, 45, Hung1.2H]. The ventilation patterns are similar with those consisting of 4 buildings. For wind direction of 0^o, air mainly enters UCL across windward street openings of O1a, O1b, O1c, and leaves UCL through leeward openings of O3a, O3b, O3c. For wind directions of 15^o, 30^o , and 45^o, air enters UCL through O1a to O1c and O2a to O2c, then leaves UCL across O2a to O2c and O4a to O4c. Age of air is relatively large and air is old in recirculation regions and downstream regions.

UCL ventilation indices and their normalized ventilation ratios (*NVR*) in all 24 test cases with 16 buildings are quantitatively analyzed, including $Q^*_{\rm roof}$ (in) and $Q^*_{\rm roof}$ (out) in Fig. 13a, $Q^*_{\rm roof}$ (turb) in Fig. 13b, Q_T^* in Fig. 13c, PFR^* in Fig. 13d and $<\tau_p^*>$ in the entire UCL in Fig. 13e. It is found that UCL ventilation indices basically become a little better if wind directions change from 0^o and 15^o to 30^o and 45^o. More importantly, roof type variations from 'Open' to 'Fully-covered' produce a large decreasing rate of overall UCL ventilation and obtain macroscopically older air, which can be represented by the below data. For roof ventilation indices(see Fig. 13a-13b), *NVR* for 'Fully-covered' type are all zero, and those for 'Partly-covered' type are 11%-23% for $Q^*_{\rm roof}$ (in), 28%-39% for $Q^*_{\rm roof}$ (out), and 16%-22% for $Q^*_{\rm roof}$ (turb). For overall UCL ventilation, *NVR* of Q_T^* (see Fig. 13c) are 81%-96% for 'Hung1.5H' type, 78%-87% for 'Hung1.2H' type, 65%-86% for 'Hung1.1H' type, 52%-61% for 'Partly-covered' type and 28%-50% for 'Fully-covered' type, and *NVR* of PFR^*(see Fig. 13d) for the above roof types are 84%-90%, 76%-87%, 65%-86%,52%-68%, and 36%-45% respectively, moreover *NVR* of $<\tau_p^*>$ increase from 111%-120%, 115%-131%, 116%-154% to 148%-192%, 223%-279% (i.e. air becomes older). Results also confirm that, 'Hung1.5H', 'Hung1.2H' and 'Hung1.1H' types produce a little smaller but comparable UCL ventilation in contrast to 'Open' type. Thus for cases with 16 buildings, the roof types of 'Hung1.2H' and 'Hung1.1H' are better choices considering they are more realistic designs.

3.4 Effect of urban size on UCL ventilation

To quantify how overall UCL ventilations change if building number or urban size increases, Fig. 13b-13e also compares $Q^*_{\rm roof}$ (turb), Q_T^*, PFR^* and $<\tau_p^*>$ between urban models with 4 or 16 buildings (the smaller or bigger model). By analyzing Fig. 13b-13d, $Q^*_{\rm roof}$

(turb), Q_T* and *PFR** in the bigger model are found several times (about 3.2-4.7 for Q^*_{roof} , 1.2-2.6 for Q_T*, 0.8-3.5 for *PFR**) larger than those in the smaller model. Larger urban model obtains greater ventilation capacity because their total area of street openings and street roofs are 2 and 5.2 times greater than the smaller one. However it does not represent larger urban model can produces better overall UCL ventilation. It can be confirmed by Fig. 13e that $< \tau_p * >$ in the bigger model is about 1.4 to 3.5 times as great as that in the smaller model, showing that the bigger model obtains macroscopically older air. It is because the bigger model has a UCL volume of 5.2 times larger than that in the smaller model and requires longer time for wind to flow through.

3.5 Discussions and Future outlooks

Further investigations are still required before formulating a practical guidelines for these semi-open street roof designs, such as the effect of the surrounding building height, the effect of atmospheric thermal stratification (not neutral) and buoyancy force due to solar shading, the analysis of rain-cover and shading capability etc. This paper is one of the first attempts to quantify and address a relationship between semi-open street roof configurations and UCL ventilation indices. The methodologies and techniques utilized in this paper are promising, and possibly provide a valid tool to investigate UCL ventilation in other types of idealized or realistic urban configurations.

4. Conclusions

The arrangements of semi-open street roofs in urban space are effective to protect pedestrians from strong sunshine and heavy rains or snows. Their effects on urban canopy layer (UCL) ventilation are still not fully understood. This paper numerically quantified how five types of semi-open street roofs influence isothermal turbulent airflows and UCL ventilation performance under a neutral atmospheric condition with various ambient wind directions (0^o,15^o, 30^o, 45^o). Two small-scale idealized urban models were investigated consisting of 4 (2×2) or 16 (4×4) buildings with uniform building height of H=0.069m, and street aspect ratio of H/W=1, corresponding to full-scale urban models of about 7m tall, 49m and 105m long as the scale ratio is 1:100. In contrast to 'Open' roof type (open street roof), five kinds of semi-open street roofs were included: Walls are hung above open street roofs (coverage ratio λ_a=100%) at z=1.1H, 1.2H, 1.5*H*, i.e. types of 'Hung1.1H', 'Hung1.2H', 'Hung1.5H'; Walls partly cover street roofs at $z=H$ (λ_a=80%), i.e. 'Partly-covered' type; Walls are set up to cover the entire street roof at $z=H$ (λ_a=100%), i.e. 'Fully-covered' type. The age of air and its spatial mean value, flow rates across street openings and street roofs, the UCL purging flow rate were numerically analyzed to quantify UCL ventilation.

Results show that the prediction of airflow velocity by using standard k-ε model agreed better with wind tunnel data than other three RANS turbulence models. Semi-open street roofs significantly influence UCL ventilation patterns and redistribute flow rates across street openings and street roofs. As roof types vary from 'Open' to 'Hung1.5H', 'Hung1.2H', 'Hung1.1H' then to 'Partly-covered' and 'Fully-covered', both roof ventilation and overall UCL ventilation performance are basically weakened. The net UCL ventilation is the worst for the 'Fully-covered' type, followed by the 'Partly-covered' type. The roof types of 'Hung1.2H' and 'Hung1.1H' are proposed because they produce comparable UCL ventilation, meanwhile are more realistic roof designs. Oblique ambient wind directions of 30^{o} and 45^{o} obtain better UCL ventilation than 15^{o} and 0^{o}. If the building number increases from 4 (2×2) to 16 (4×4), air in the entire UCL becomes macroscopically older because the greater UCL volume requires longer time for rural wind to flow through.

Acknowledgements

This study was financially supported by the National Natural Science Foundation of China (No. 51108102) and Guangdong Natural Science Foundation (Code S2011040004149). The two anonymous reviewers who provided constructive suggestions and comments are also gratefully acknowledged.

Nomenclature

A	area of a surface (m^2)
B, H, L, W	building width, building height, total length, street width
$\bar{c}, <\bar{c}>$	time-averaged pollutant concentration(kgm^{-3}) and its spatial mean value
K_c, ν_t	turbulent eddy diffusivity of pollutant and momentum $K_c = \nu_t / S_{ct}$
k, ε	turbulent kinetic energy and its dissipation rate

$\vec{n}$	normal direction of street openings or canopy roofs
NVR	normalized ventilation ratio in contrast to models with 'open' street roofs
PFR,*PFR**	purging flow rate and its normalized value ($PFR^*=PFR/Q_\infty$)
Q^*	normalized flow rate through street openings or street roofs
Q_{in}^*, Q_{out}^*	normalized total inflow and outflow rate for entire UCL
Q_T^*	total ventilation flow rate by mean flows (m^3s^{-1})
Q_∞	reference flow rate in upstream free flow to normalize flow rates
Q^*_{roof} (turb)	normalized effective flow rate across street roofs by turbulence
Q^*_{roof} (in)	normalized inflow rate across street roofs by downward flows
Q^*_{roof} (out)	normalized outflow rate across street roofs by upward outflows
S_c	pollutant release rate
S_{ct}	turbulent Schmidt number
σ_w	fluctuation velocity on street roofs
τ_p, τ_p^*	age of air (s) and its normalized value
$<\tau_p^*>$	normalized spatial mean age of air
U_m, I_m	velocity, turbulence intensity measured in upstream free flow
$U_0(z)$	velocity profiles used at CFD domain inlet for ventilation cases
U_H	reference velocity (2.66m/s) at $z=H$
$\bar{u}_j$, x_j	velocity and coordinate components
$\vec{V}$	velocity vector
Vol	control volume
x, *y*, *z*	stream-wise, span-wise, vertical directions

References

[1] Oke TR. Street design and urban canopy layer climate. Energ Build 1988; 11(1-3): 103-113.

[2] Bady M, Kato S, Huang H. Towards the application of indoor ventilation efficiency indices to evaluate the air quality of urban areas. Build Environ 2008; 43(12): 1991-2004.

[3] Deng Q, He G, Lu C, Liu W. Urban ventilation - a new concept and lumped model. Int J Vent 2012; 11: 131-140.

[4] Yang, XY, Li YG, Yang LN. Predicting and understanding temporal 3D exterior surface temperature distribution in an ideal courtyard. Build Environ 2012; 57:38-48.

[5] Kato S, Murakami S, Takahashi T, Gyobu T. Chained analysis of wind tunnel test and CFD on cross ventilation of large-scale market building. J Wind Eng Ind Aerodyn 1997; 67-68: 573-587.

[6] da Graça GC, Martins NR, Horta CS. Thermal and airflow simulation of a naturally ventilated shopping mall. Energ Build 2012; 50: 177-188.

[7] Kim T, Kim K, Kim BS. A wind tunnel experiment and CFD analysis on airflow performance of enclosed-arcade markets in Korea. Build Environ 2010; 45: 1329-1338.

[8] Hang J, Li Y, Sandberg M, Buccolieri R, Di Sabatino S. The influence of building height variability on pollutant dispersion and pedestrian ventilation in idealized high-rise urban areas. Build Environ 2012; 56: 346-360.

[9] Hu T, Yoshie R. Indices to evaluate ventilation efficiency in newly-built urban area at pedestrian level. J Wind Eng Ind Aerodyn 2013; 112: 39–51.

[10]Buccolieri R, Sandberg M, Di Sabatino S. City breathability and its link to pollutant concentration distribution within urban-like geometries. Atmos Environ 2010; 44(15): 1894-1903.

[11]Hang J, Li Y, Buccolieri R, Sandberg M, Di Sabatino S. On the contribution of mean flow and turbulence to city breathability: the case of long streets with tall buildings. Sci Total Environ 2012; 416: 363-373.

[12]Britter RE, Hanna SR. Flow and dispersion in urban areas. Annu Rev Fluid Mech 2003; 35:469-496.

[13] Arnfield AJ. Two decades of urban climate research: a review of turbulence, exchanges of energy and water, and the urban heat island. Int J Climato 2003; 23:1-26.

[14] Grimmond CSB, Blackett M, Best MJ, Barlow J, Baik JJ, Belcher SE et al. The International Urban Energy Balance Models Comparison Project: First Results from Phase 1. J Appl Meteorol Clim 2010; 49: 1268-1292.

[15] Li XX, Liu CH, Leung DYC, Lam KM. Recent progress in CFD modelling of wind field and pollutant transport in street canyons. Atmos Environ 2006; 40(29): 5640-5658.

[16] Meroney RN, Pavegeau M, Rafailidis S, Schatzmann M. Study of line source characteristics for 2-D physical modelling of pollutant dispersion in street canyons. J Wind Eng Ind Aerodyn 1996; 62(1):37-56.
[17] Li XX, Liu CH, Leung DYC. Numerical investigation of pollutant transport characteristics inside deep urban street canyons. Atmos Environ 2009; 43(15): 2410-2418.
[18] Salim SM, Cheah SC, Chan A. Numerical simulation of dispersion in urban street canyons with avenue-like tree plantings: Comparison between RANS and LES. Build Environ 2011; 46(9): 1735-1746.
[19] Cai XM. Effects of differential wall heating in street canyons on dispersion and ventilation characteristics of a passive scalar. Atmos Environ 2012; 51: 268-277.
[20] Di Sabatino S, Buccolieri R, Pulvirenti B, Bitter R. Simulations of pollutant dispersion within idealised urban-type geometries with CFD and integral models. Atmos Environ 2007; 41(37):8316-8329.
[21] Kanda M. Large-eddy simulations on the effects of surface geometry of building arrays on turbulent organized structures. Boundary-layer meteorol 2006; 18(1): 151-168.
[22] Zaki SA, Hagishima A, Tanimoto J, Ikegaya N. Aerodynamic Parameters of Urban Building Arrays with Random Geometries. Boundary-Layer Meteorol 2011; 138:99-120.
[23] Abd Razak A, Hagishima A, Ikegaya N, Tanimoto J. Analysis of airflow over building arrays for assessment of urban wind environment. Build Environ 2013; 59:56-65.
[24] Yim SHL, Fung JCH, Lau AKH, Kot SC. Air ventilation impacts of the "wall effect" resulting from the alignment of high-rise buildings. Atmos Environ 2009; 43(32): 4982-4994.
[25] Hagishima A, Tanimoto J, Nagayama K, Meno S. Aerodynamic parameters of regular arrays of rectangular blocks with various geometries. Boundary-Layer Meteorol 2009; 132(2):315-337.
[26] Gu ZL, Zhang YW, Cheng Y, Lee SC. Effect of uneven building layout on air flow and pollutant dispersion in non-uniform street canyons. Build Environ 2011; 46(12): 2657-2665.
[27] Chen Q. Ventilation performance prediction for buildings: a method overview and recent applications. Build Environ 2009; 44:848-858.
[28] Luo ZW, Li YG. Passive urban ventilation by combined buoyancy-driven slope flow and wall flow: Parametric CFD studies on idealized city models. Atmos Environ 2011; 45(32):5946-5956.

[29] Yang LN, Li YG. Thermal conditions and ventilation in an ideal city model of Hong Kong. Energ Buildings 2011; 43(5): 1139-1148.

[30]Hang J, Li YG. Wind conditions in idealized building clusters--macroscopic simulations by a porous turbulence model. Boundary-Layer Meteorol 2010; 136(1): 129-159.

[31]Liu CH, Cheng WC , Leung TCY, Leung DYC. On the mechanism of air pollutant re-entrainment in two-dimensional idealized street canyons. Atmos Environ 2011; 45(27) : 4763-4769.

[32] Hang J, Sandberg M, Li YG. Age of air and air exchange efficiency in idealized city models. Build Environ 2009; 44(8):1714-1723.

[33]Santiago JL, Dejoan A, Martilli A, Martin F, Pinelli A. Comparison between Large-Eddy Simulation and Reynolds-Averaged Navier–Stokes computations for the MUST field experiment. Part I: study of the flow for an incident wind directed perpendicularly to the front array of containers. Boundary-Layer Meteorol 135; 2010:109-132.

[34] Salim SM, Buccolieri R, Chan A, Di Sabatino S. Numerical simulation of atmospheric pollutant dispersion in an urban street canyon: Comparison between RANS and LES. J Wind Eng Ind Aerodyn 2011; 99(2-3): 103-113.

[35] Yoshie R, Mochida A, Tominaga Y, Kataoka H, Harimoto K, Nozu T, Shirasawa T. Cooperative project for CFD prediction of pedestrian wind environment in the Architectural Institute of Japan. J Wind Eng Ind Aerodyn 2007; 95:1551-1578.

[36] Mochida A, Lun IYF. Prediction of wind environment and thermal comfort at pedestrian level in urban area. J Wind Eng Ind Aerodyn 2008; 96(10-11): 1498-1527.

[37]Hang J, Sandberg M, Li Y. Effect of urban morphology on wind condition in idealized city models. Atmos Environ 2009; 43(4): 869-878.

[38] FLUENT V6.3. User's Manual.2006. http://www.fluent.com.

[39] Snyder WH. Similarity criteria for the application of fluid models to the study of air pollution meteorology. Boundary-Layer Meteorol 1972; 3:113-134.

[40] Tominaga Y, Mochida A, Yoshie R, Kataoka H, Nozu T, Yoshikawa M, Shirasawa T. AIJ guidelines for practical applications of CFD to pedestrian wind environment around buildings. J Wind Eng Ind Aerodyn 2008; 96(10-11):1749-1761.

[41] Lien FS, Yee E. Numerical modelling of the turbulent flow developing within and over a 3-D building array, part I: A high-resolution Reynolds-averaged Navier-Stokes approach. Boundary-layer Meteorol 2004; 112(3): 427-466.

[42] Irwin JS. A theoretical variation of the wind profile power-law exponent as a function of surface roughness and stability. Atmos Environ 1979**;** 13(1):191-194.

[43]WMO Guide to Meteorological Instruments and Methods of Observation WMO-No. 8, page I.5-12

[44]Etheridge D, Sandberg M. Building Ventilation: Theory and Measurement. John Wiley & Sons, Chichester. 1996, p.573-633.

[45] Tominaga Y, Stathopoulos T. Turbulent Schmidt numbers for CFD analysis with various types of flow field. Atmos Environ 2007; 41(37):8091-8099.

Figure list

Fig. 1. Two urban configurations of semi-open street roof design: (a) Walls being hung above street roofs of food court, (b) Walls being partly covered at street roof height (*z*=*H*) of retail center.

Fig. 2. Model descriptions of experimental model: (a) The idealized urban model with 4 buildings and open street roof, (b) Vertical profiles of velocity and turbulence intensity in the upstream free flow of wind tunnel experiment.

Fig. 3. (a) Computational domain for cases with a parallel approaching wind (0^o)and half domain size, (b) Grid arrangements in *x*-*y* plane in the validation case.

Fig. 4. (a) Computational domain with oblique wind direction and full domain size. Model descriptions of urban models with (b) 4 (2×2) buildings and (c) 16 (4×4) buildings.

Fig. 5. (a)'Fully-covered' roof type: walls fully cover street roofs at *z*=*H* (b) 'Partly-covered' roof type: walls partly cover street roofs at *z*=*H*, (c) Types of 'Hung1.5H', 'Hung1.2H', 'Hung1.1H': walls are hung above street roofs at *z*=1.1*H*, 1.2*H*, 15*H*.

Fig. 6. Two examples of grid arrangements for urban geometries with 4 buildings: (a) in *x*-*y* plane, (b) in *x*-*z* plane. (c)Definition of uniform pollutant source in UCL volume.

Fig. 7. Validation profiles of (a) velocity and (b) turbulence intensity along the street centerline at z=0.11H by using different turbulence models. (c) Horizontal profiles of velocity for a grid independence study.

Fig. 8. (a) 3D streamline, (b) τ_p* in z=0.22H and $Q*$ in Case [2-2, 0, Open], Case [2-2, 0, Hung1.2H], Case [2-2, 0, Partly-covered], Case [2-2, 0, Fully-covered].

Fig. 9. (a) 3D streamline, (b) τ_p* and $Q*$ in Case [2-2, 0, Hung1.5H], Case [2-2, 15, Hung1.5H], Case [2-2, 30, Hung1.5H], Case [2-2, 45, Hung1.5H]. Note that in Fig. 9b, negative values of $Q*$ by mean flows denote air leaving UCL and positive ones represent air entering UCL.

Fig. 10. $Q*$ in urban models with 4 buildings and wind directions of (a) 0^o, (b) 15^o, (c) 30^o, (d)45^o.

Fig. 11. Ventilation indices and their *NVR* for test cases with 4 buildings: (a) $Q*_{roof}$ (in) and $Q*_{roof}$ (out), (b) $Q*_{roof}$ (turb), (c) Q_T*, (d) $PFR*$, (e) $<\tau_p*>$.

Fig. 12. τ_p* in z=0.22H in (a) Case [4-4, 0, Hung1.2H], (b) Case [4-4, 15, Hung1.2H], (c) Case [4-4, 30, Hung1.2H], (d) Case [4-4, 45, Hung1.2H].

Fig. 13. Ventilation indices and their *NVR*: (a) $Q*_{roof}$ (in) and $Q*_{roof}$ (out) in 24 test cases with 16 buildings, In all 48 test cases: (b) $Q*_{roof}$ (turb), (c) Q_T*, (d) $PFR*$, (e) $<\tau_p*>$.

Table 1 Model descriptions of 48 test cases.

2 rows, 2 columns (2×2)		4 rows, 4 columns (4×4)	
Case name*	Ambient wind direction θ^o	Case name	Ambient wind direction θ^o
[2-2, 0, Open]	0^o	[4-4, 0, Open]	0^o
[2-2, 0, Hung1.5H]		[4-4, 0, Hung1.5H]	
[2-2, 0, Hung1.2H]		[4-4, 0, Hung1.2H]	
[2-2, 0, Hung1.1H]		[4-4, 0, Hung1.1H]	
[2-2, 0,Partly-covered]		[4-4, 0,Partly-covered]	
[2-2, 0, Fully-covered]		[4-4, 0, Fully-covered]	
[2-2, 15, Open]	15^o	[4-4, 15, Open]	15^o
[2-2, 15, Hung1.5H]		[4-4, 15, Hung1.5H]	
[2-2, 15, Hung1.2H]		[4-4, 15, Hung1.2H]	
[2-2, 15, Hung1.1H]		[4-4, 15, Hung1.1H]	
[2-2, 15,Partly-covered]		[4-4, 15,Partly-covered]	
[2-2, 15, Fully-covered]		[4-4, 15, Fully-covered]	
[2-2, 30, Open]	30^o	[4-4, 30, Open]	30^o
[2-2, 30, Hung1.5H]		[4-4, 30, Hung1.5H]	
[2-2, 30, Hung1.2H]		[4-4, 30, Hung1.2H]	
[2-2, 30, Hung1.1H]		[4-4, 30, Hung1.1H]	
[2-2, 30,Partly-covered]		[4-4, 30,Partly-covered]	
[2-2, 30, Fully-covered]		[4-4, 30, Fully-covered]	
[2-2, 45, Open]	45^o	[4-4, 45, Open]	45^o
[2-2, 45, Hung1.5H]		[4-4, 45, Hung1.5H]	
[2-2, 45, Hung1.2H]		[4-4, 45, Hung1.2H]	
[2-2, 45, Hung1.1H]		[4-4, 45, Hung1.1H]	
[2-2, 45,Partly-covered]		[4-4, 45,Partly-covered]	
[2-2, 45, Fully-covered]		[4-4, 45, Fully-covered]	

*Case name is defined as [row number-column number, wind direction (θ^o), roof type]. Open' denotes open street roofs; 'Fully-covered' and 'Partly-covered' means solid walls 'fully or 'partly cover' street roofs at $z=H$. 'Hung1.5H, Hung1.2H and Hung1.1H' represent solid walls are 'Hung' above street roofs at z=1.5H, 1.2H and 1.1H.

Table 2 Effect of turbulence models and turbulent Schimdt number (*Sct*) on $<\tau_p*>$, *PFR** and Q_T* in the entire UCL, Q_{roof}(turb)* and *Q** across O3 in Case [2-2, 0, Open].

Turbulence models	Sct	$<\tau_p*>$	*PFR**	Q_T*	$Q*_{roof}$(out)	$Q*_{roof}$(in)	$Q*_{roof}$(turb)	*Q**(O3)
Standard k-ε	0.4	21.2	1.847	1.376	-0.825	0.148	1.211	-0.551
	0.7	24.3	1.609					
	1.0	26.4	1.482					
Realizable k-ε	0.7	27.2	1.439	1.401	-0.844	0.145	1.066	-0.536
RNG k-ε	0.7	28.8	1.358	1.378	-1.127	0.181	0.919	-0.274

*Negative values denote air leaving UCL and positive ones represent air entering it.

(a)

(b)

Fig. 1. Hang et al.

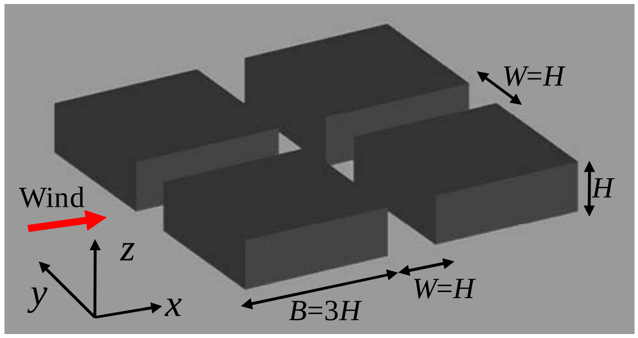

(a)

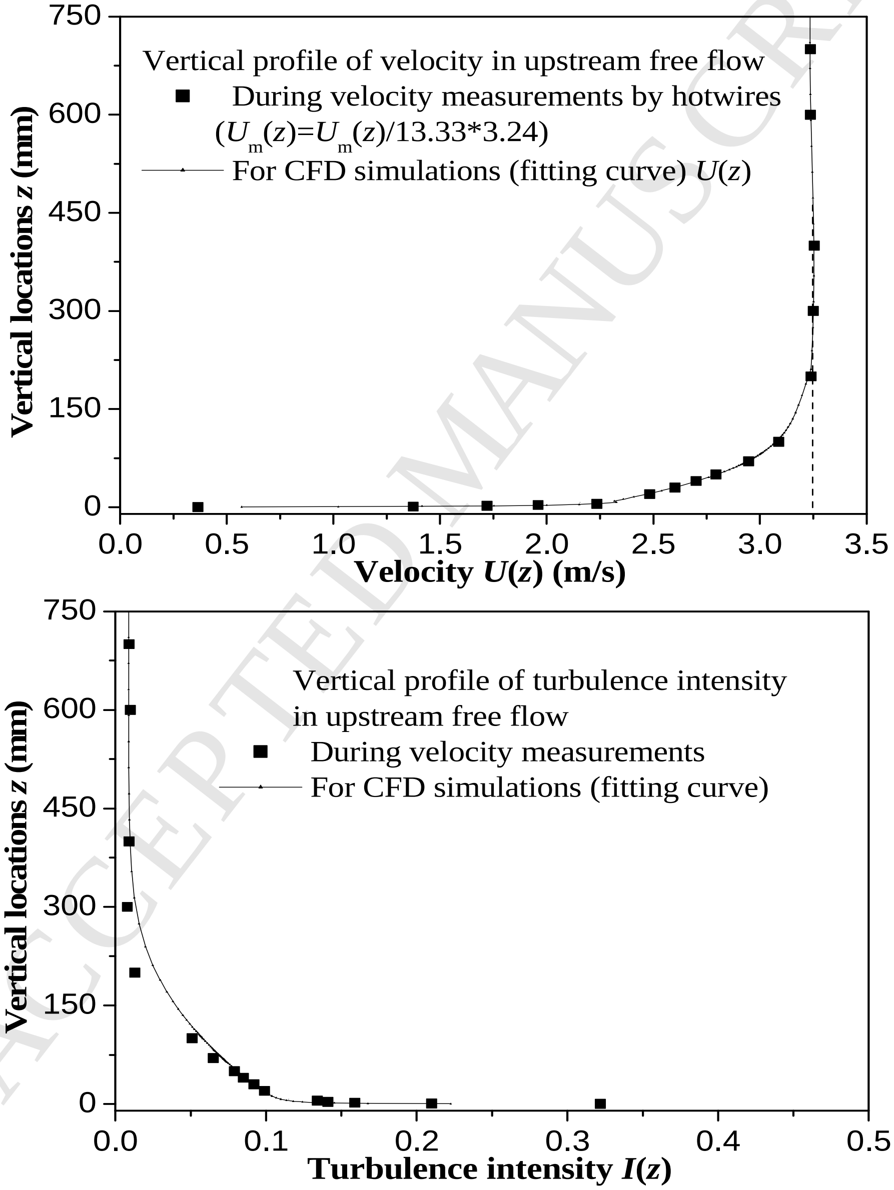

(b)

Fig. 2. Hang et al.

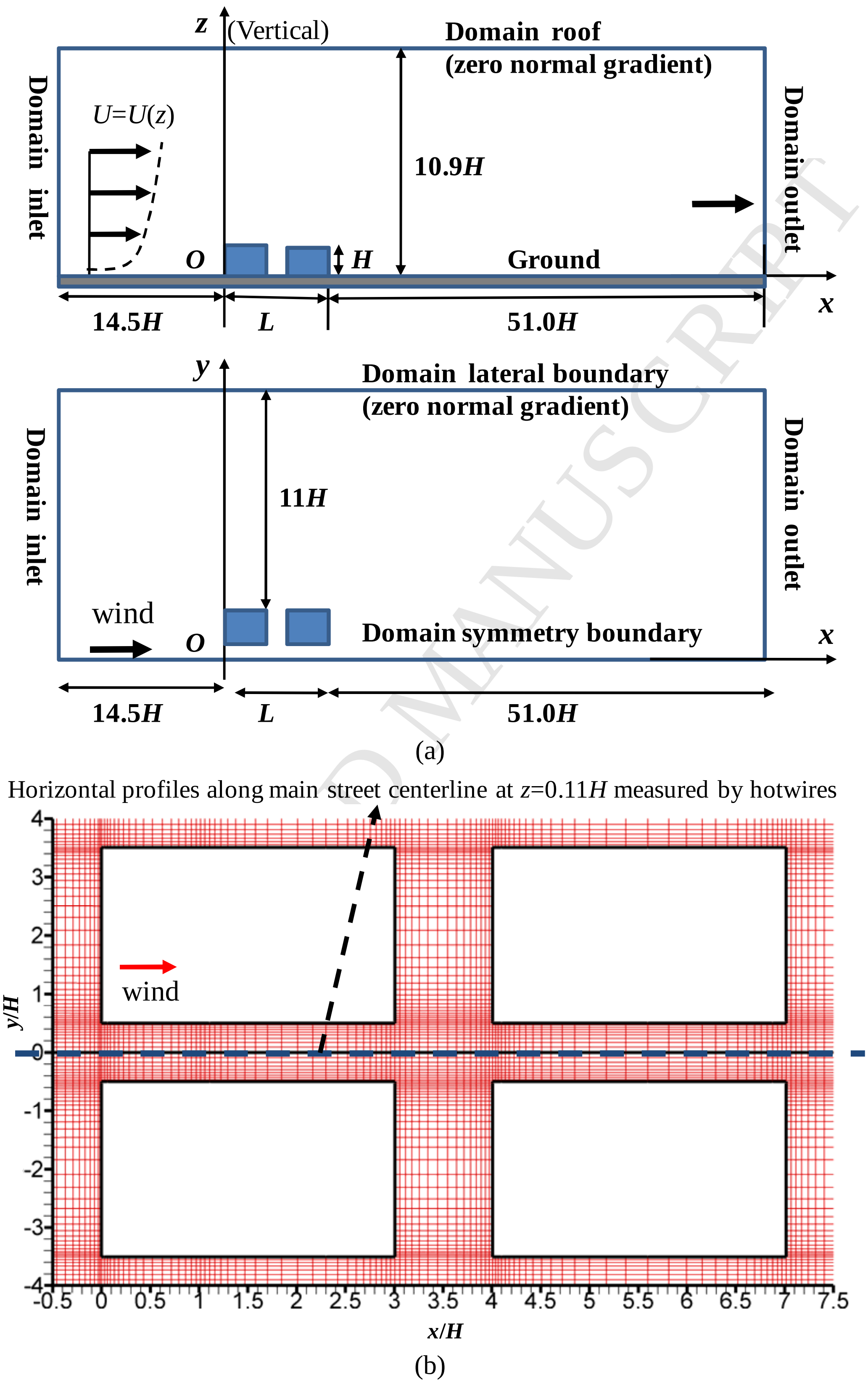

Fig. 3 Hang et al.

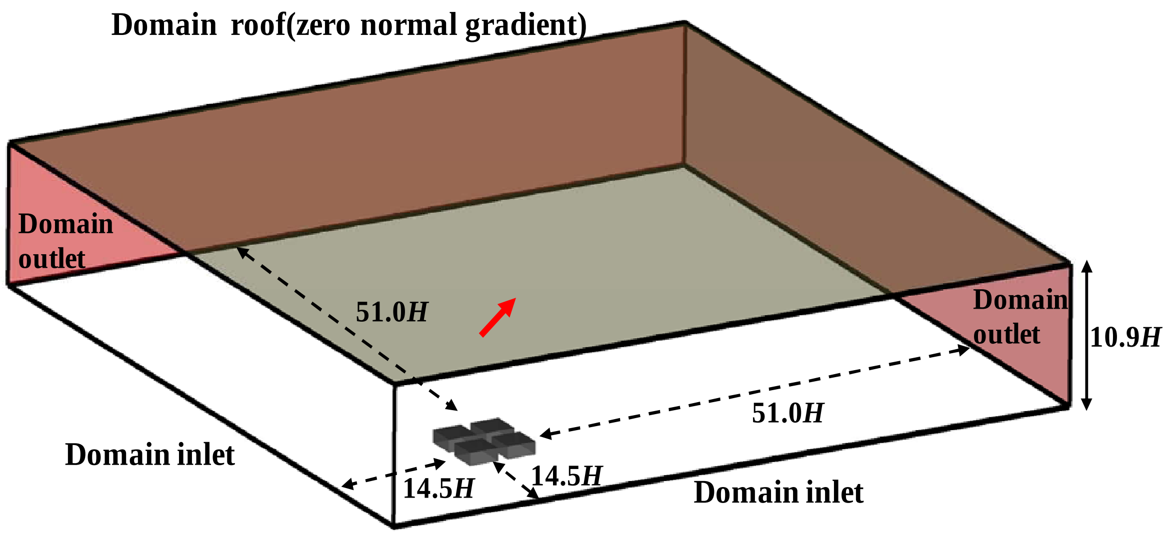
Domain roof(zero normal gradient)
Domain
outlet
51.0H
Domain
outlet
10.9H
51.0H
Domain inlet
14.5H
14.5H
Domain inlet

(a)

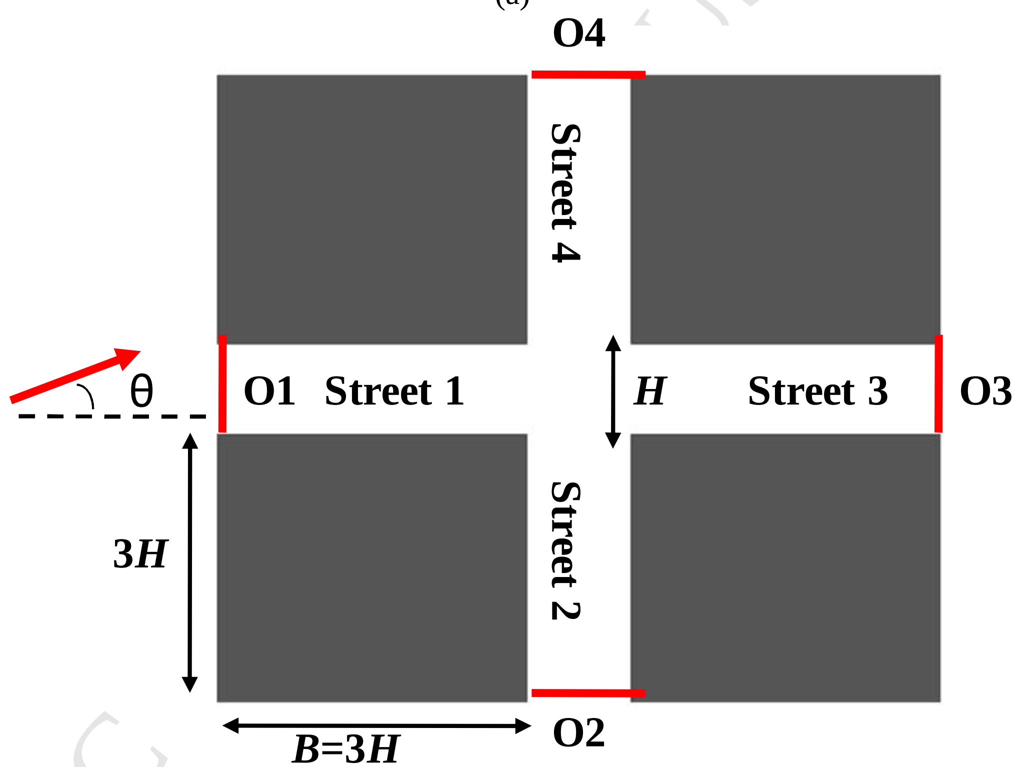
O4
Street 4
θ
O1 Street 1
H
Street 3
O3
3H
Street 2
B=3H
O2

(b)

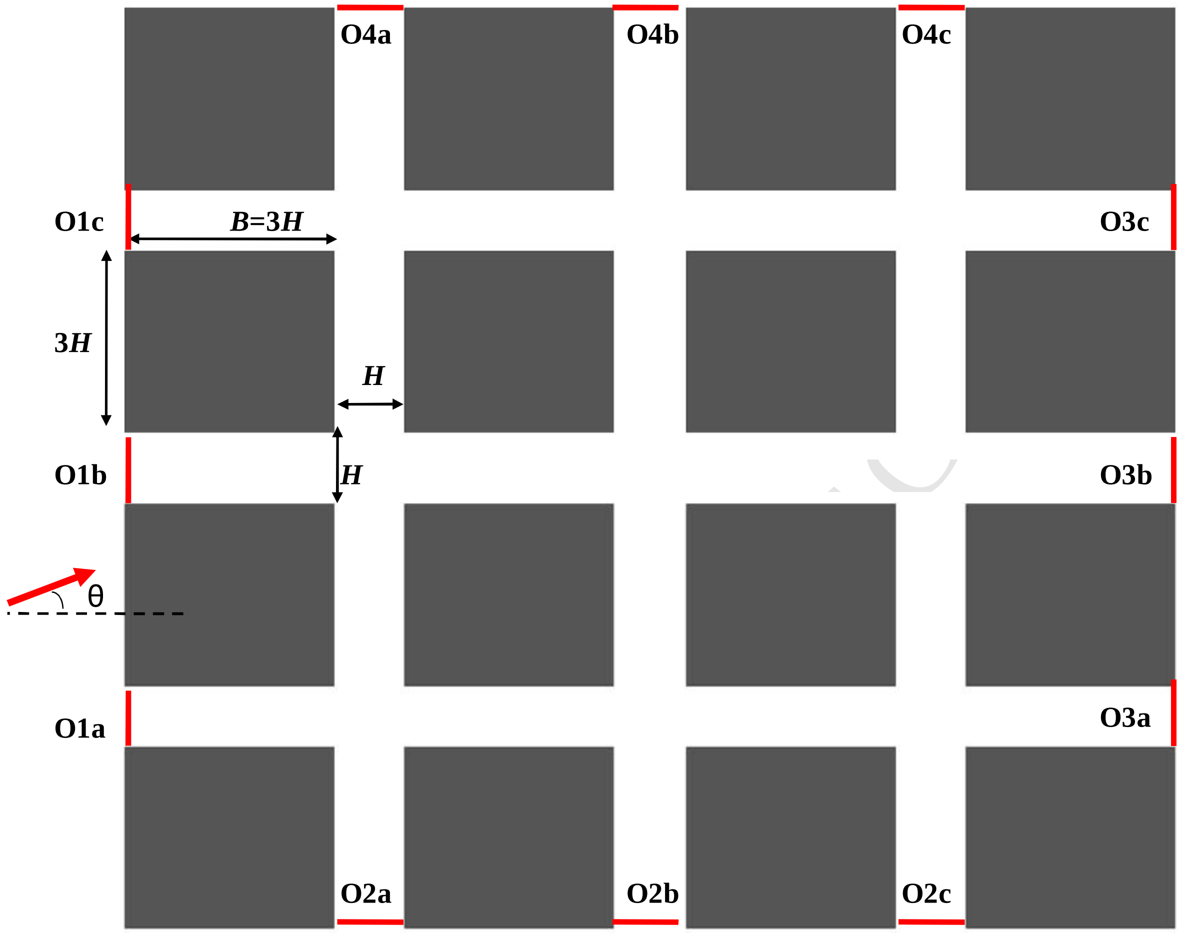

(c)

Fig. 4. Hang et al.

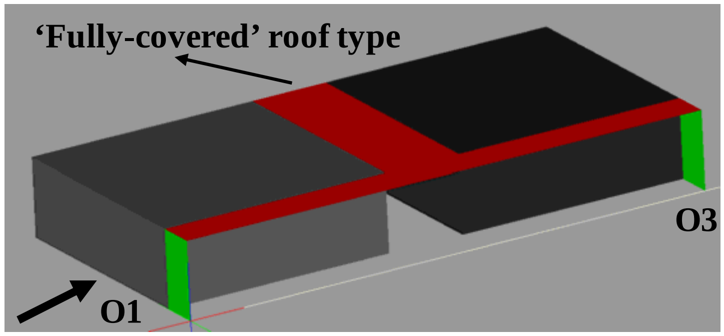

(a) Enclosed street roof

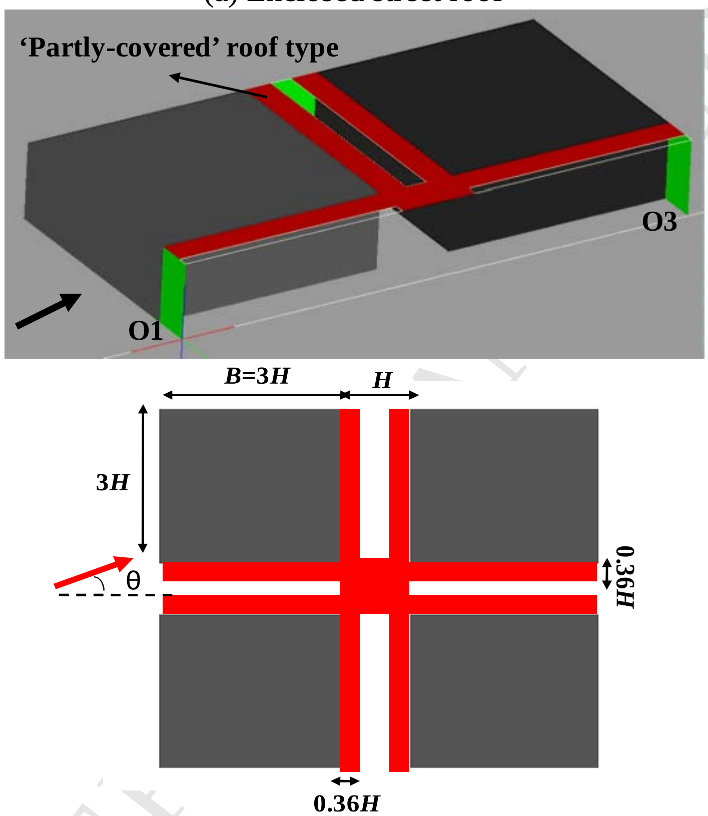

(b)

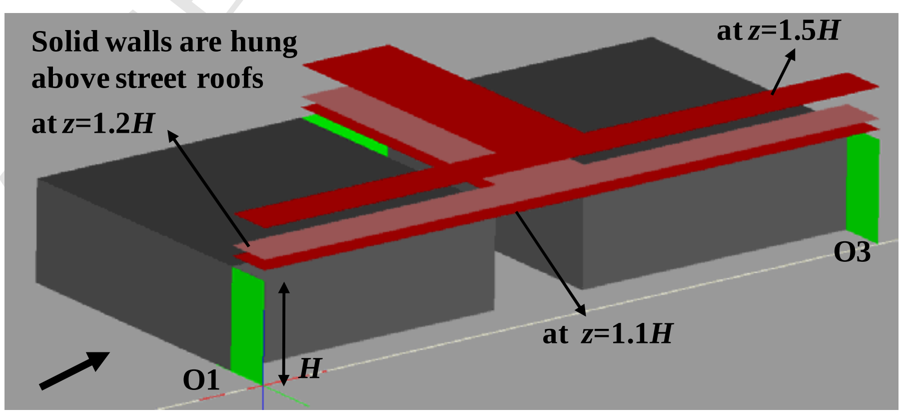

(c)

Fig. 5. Hang et al.

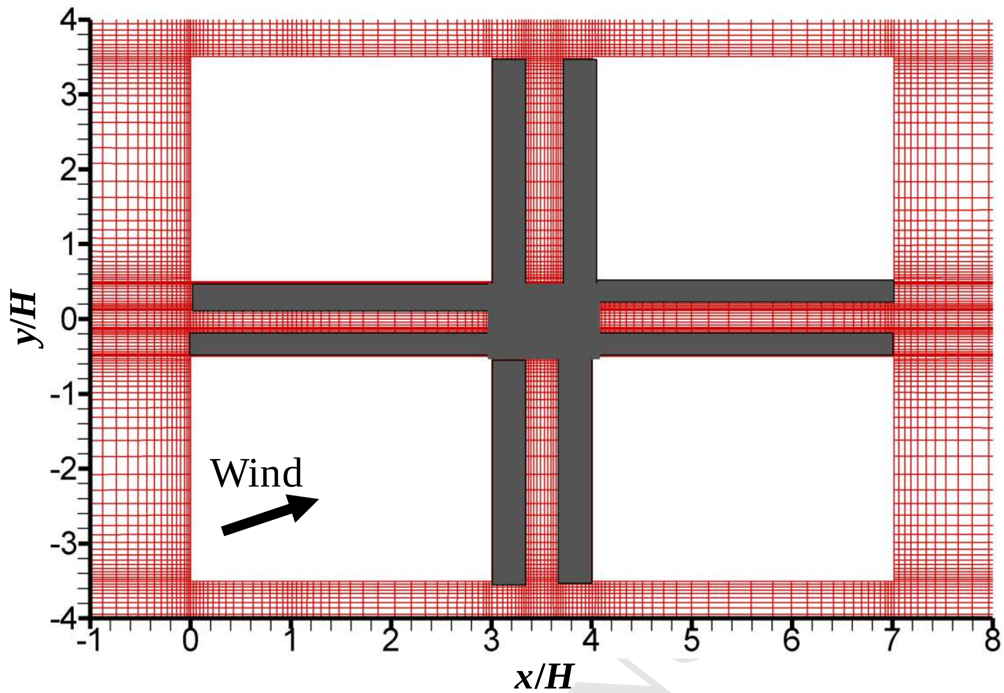

(a)

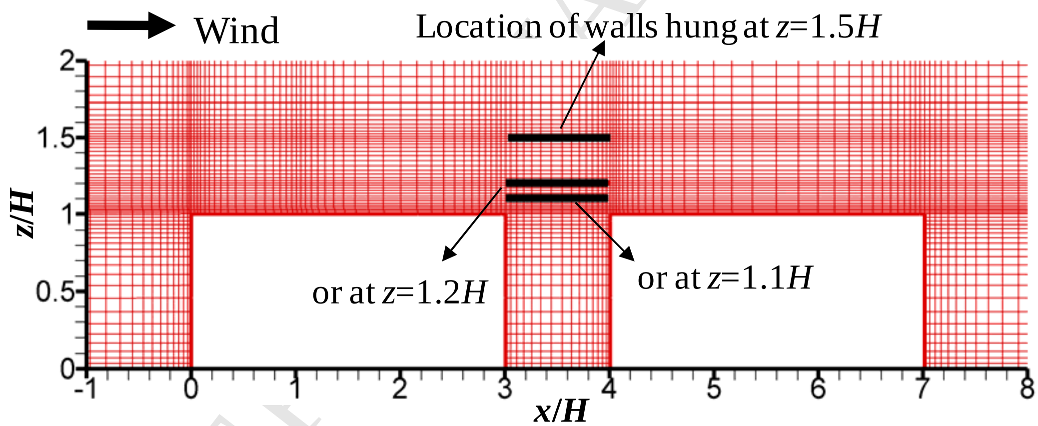

(b)

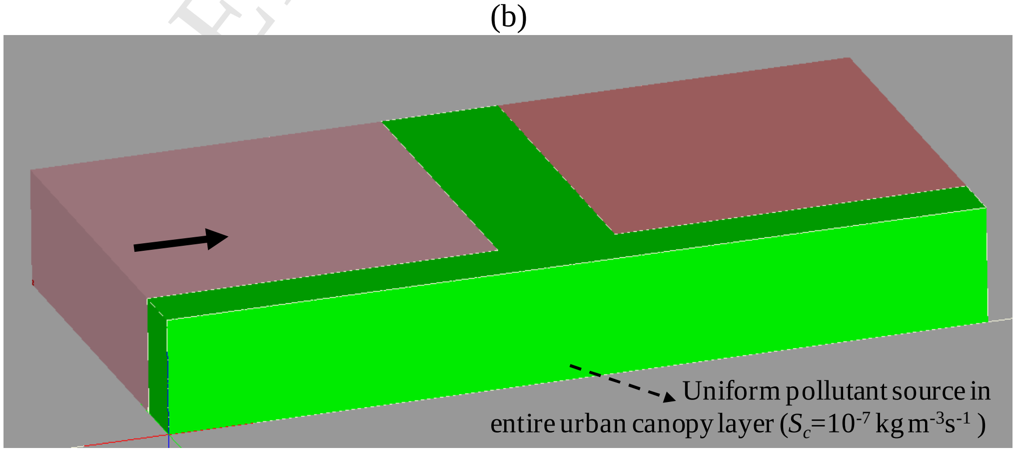

(c)

Fig.6. Hang et al.

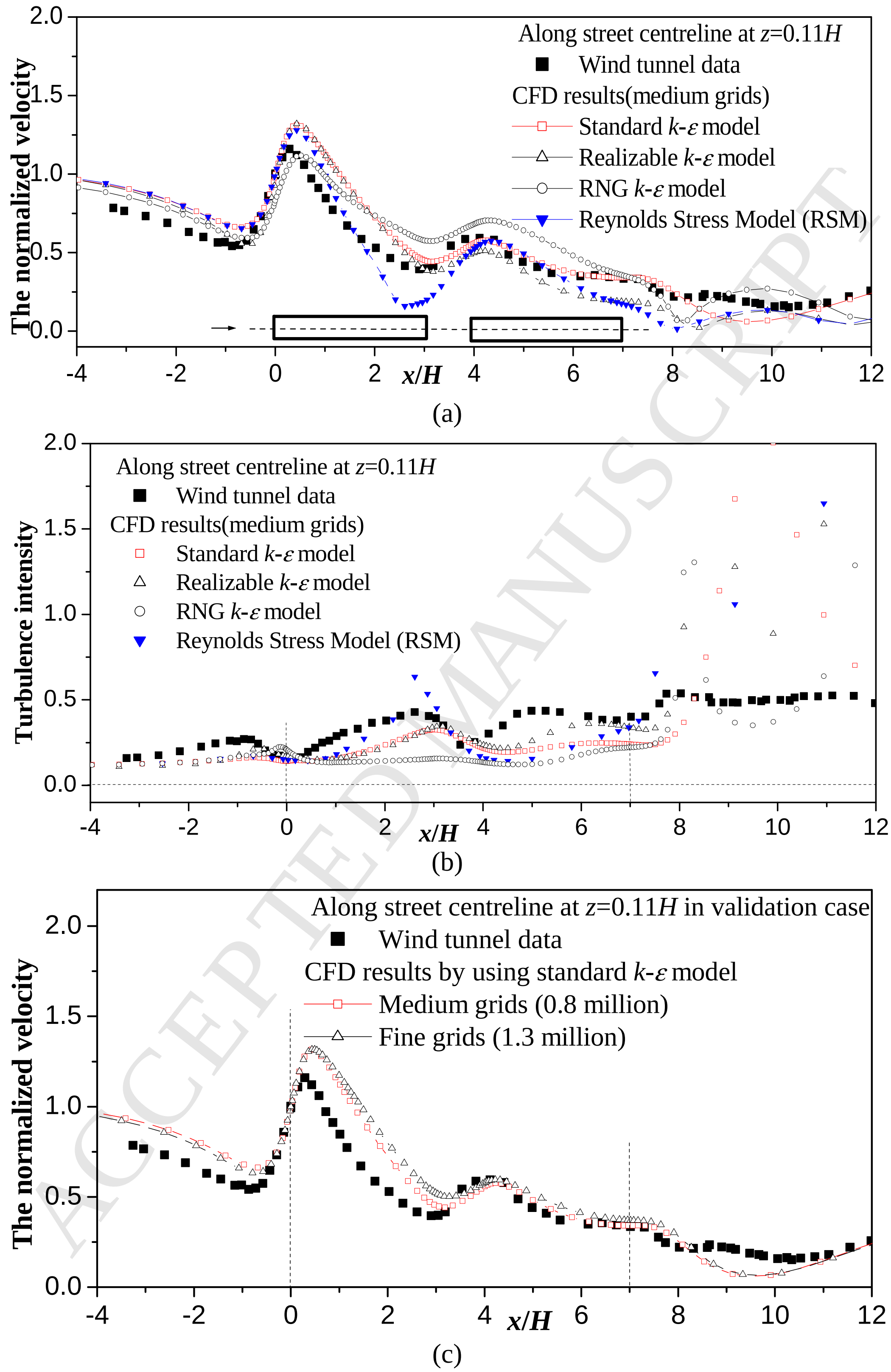

Fig. 7. Hang et al.

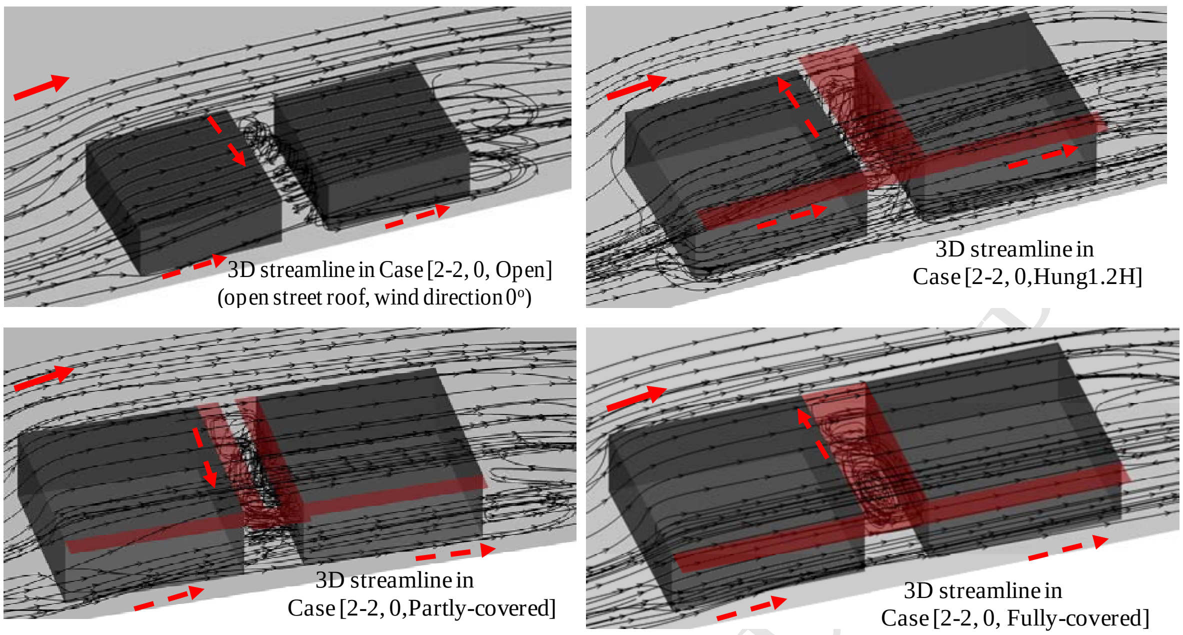

(a)

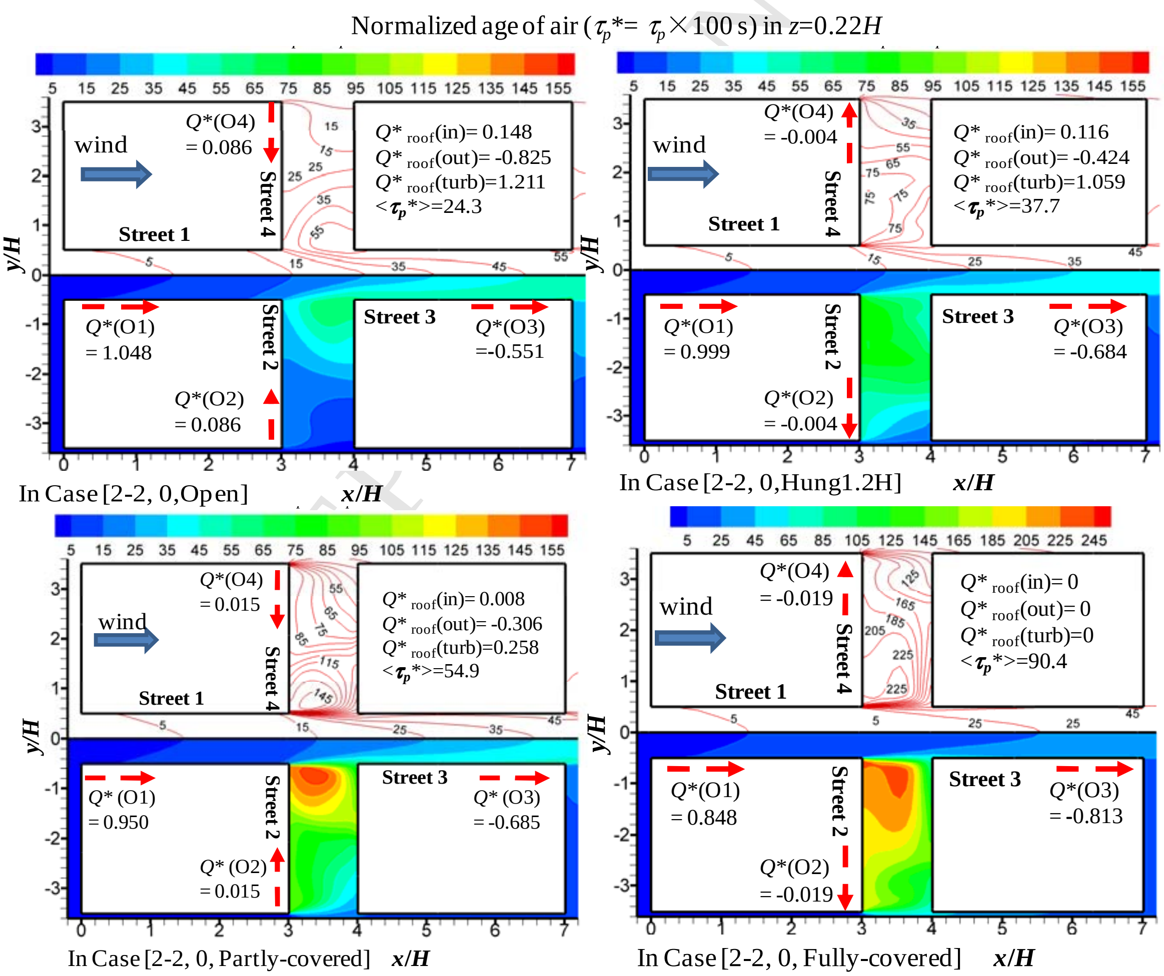

(b)

Fig. 8 Hang et al.

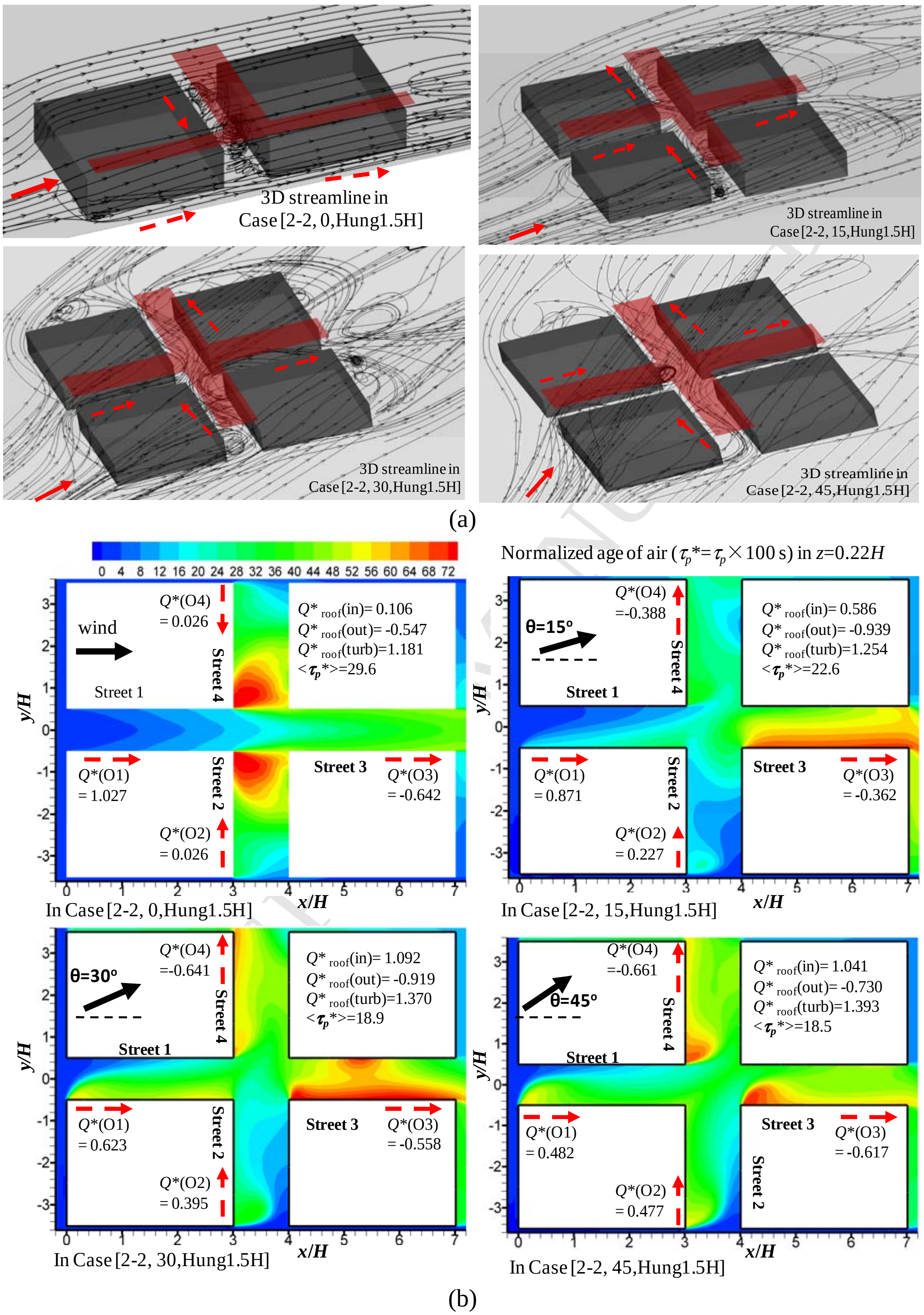

Fig. 9 Hang et al.

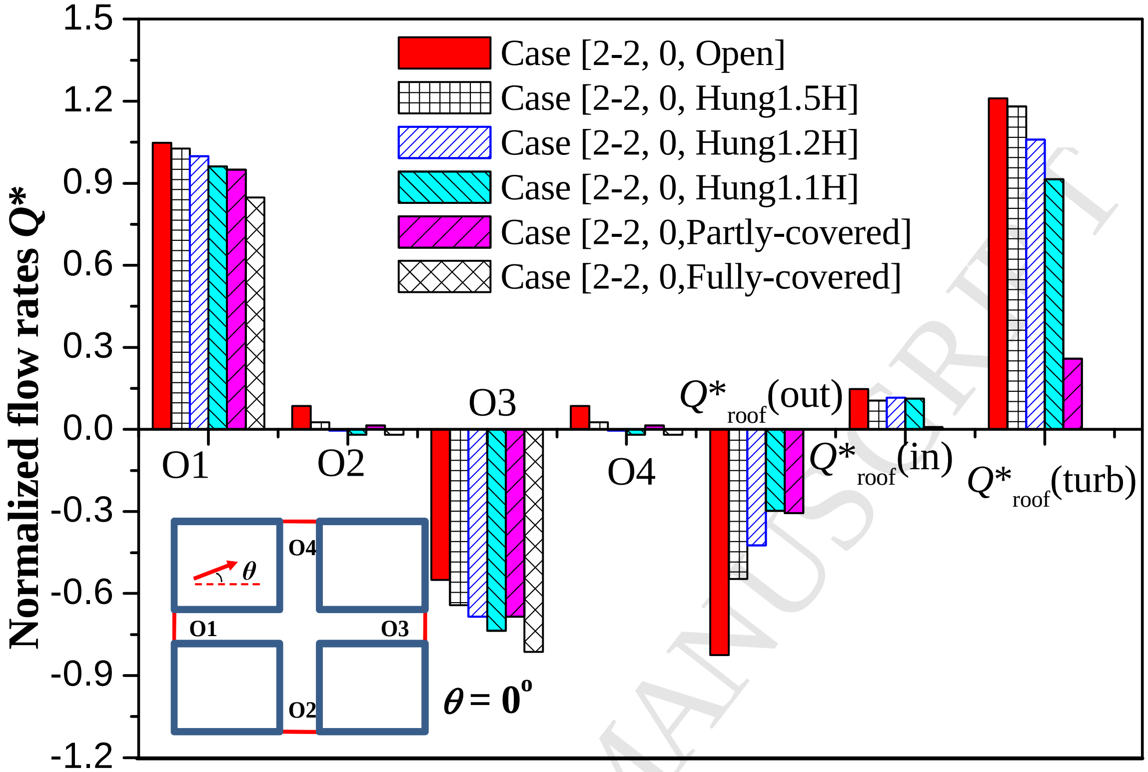
Normalized flow rates Q*
1.5
1.2
0.9
0.6
0.3
0.0
-0.3
-0.6
-0.9
-1.2
Case [2-2, 0, Open]
Case [2-2, 0, Hung1.5H]
Case [2-2, 0, Hung1.2H]
Case [2-2, 0, Hung1.1H]
Case [2-2, 0,Partly-covered]
Case [2-2, 0,Fully-covered]
O1
O2
O3
O4
Q*roof(out)
Q*roof(in)
Q*roof(turb)
O4
O1
O3
O2
θ
θ = 0°

(a)

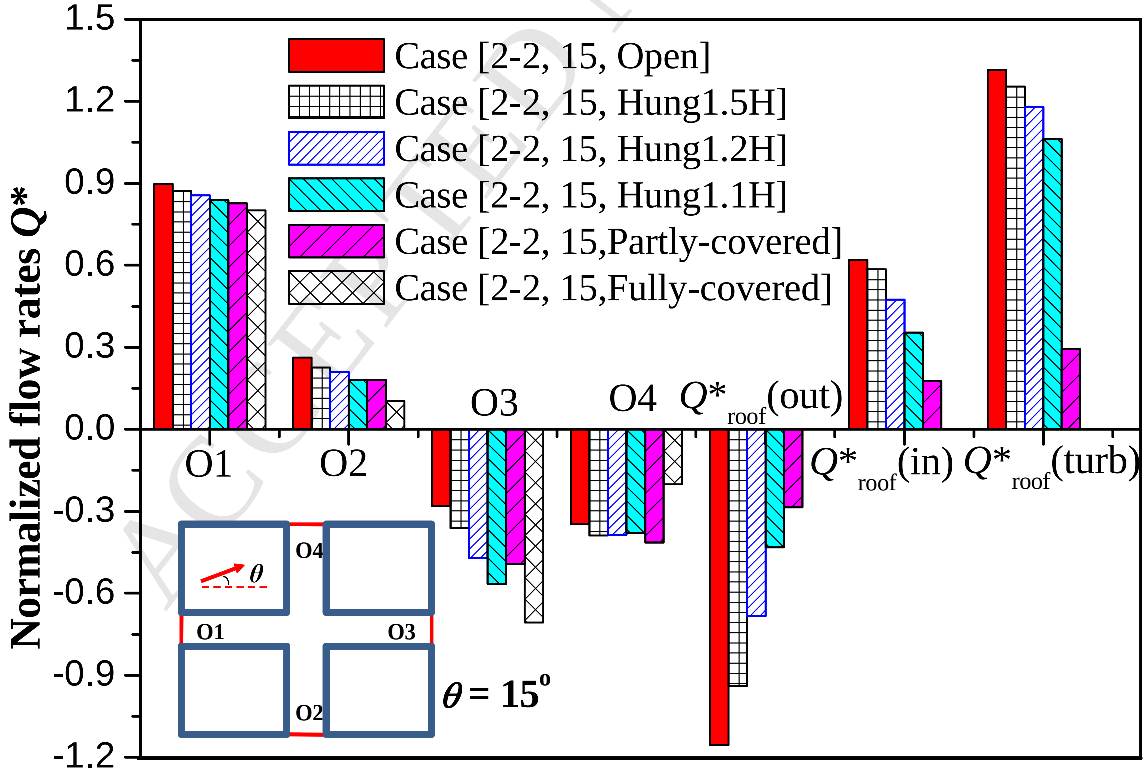
Normalized flow rates Q*
1.5
1.2
0.9
0.6
0.3
0.0
-0.3
-0.6
-0.9
-1.2
Case [2-2, 15, Open]
Case [2-2, 15, Hung1.5H]
Case [2-2, 15, Hung1.2H]
Case [2-2, 15, Hung1.1H]
Case [2-2, 15,Partly-covered]
Case [2-2, 15,Fully-covered]
O1
O2
O3
O4
Q*roof(out)
Q*roof(in)
Q*roof(turb)
O4
O1
O3
O2
θ
θ = 15°

(b)

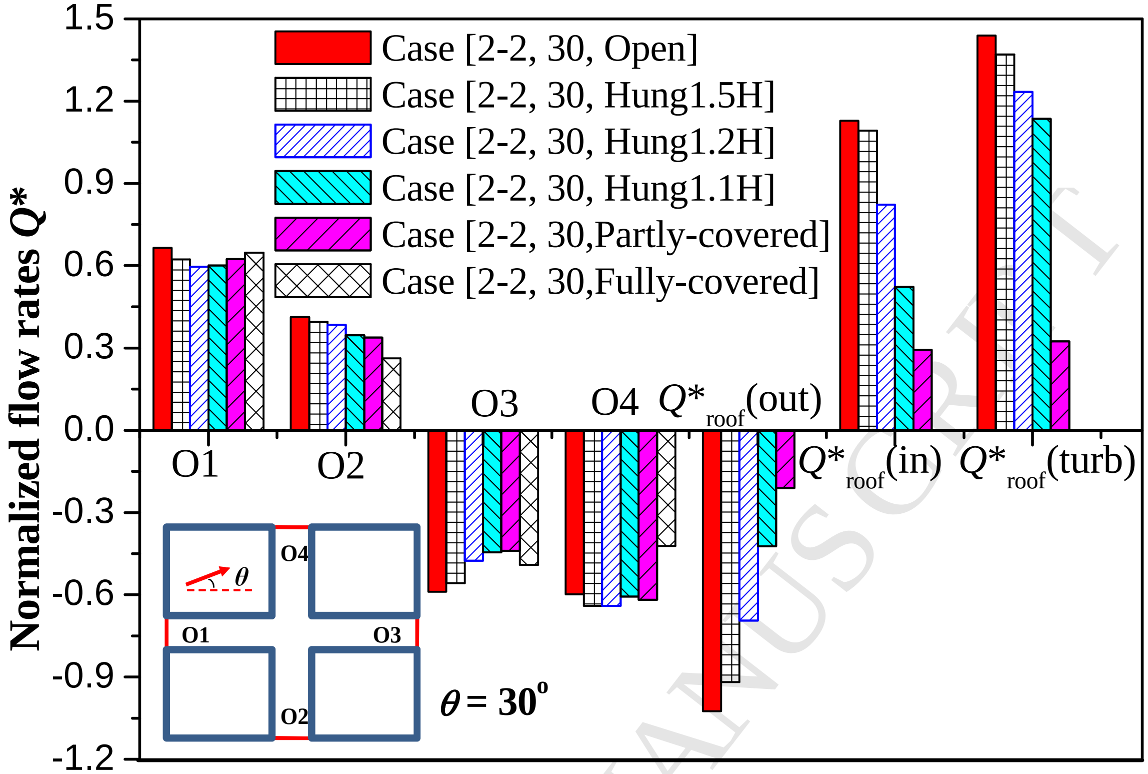

(c)

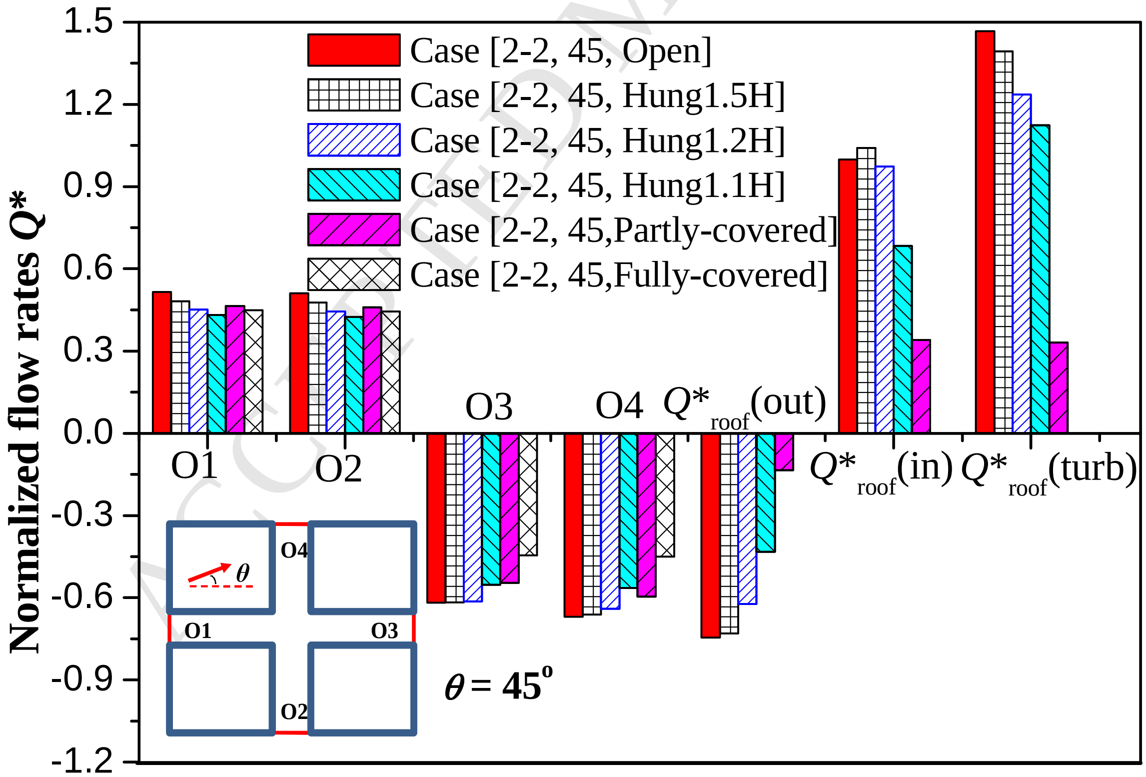

(d)

Fig.10 . Hang et al.

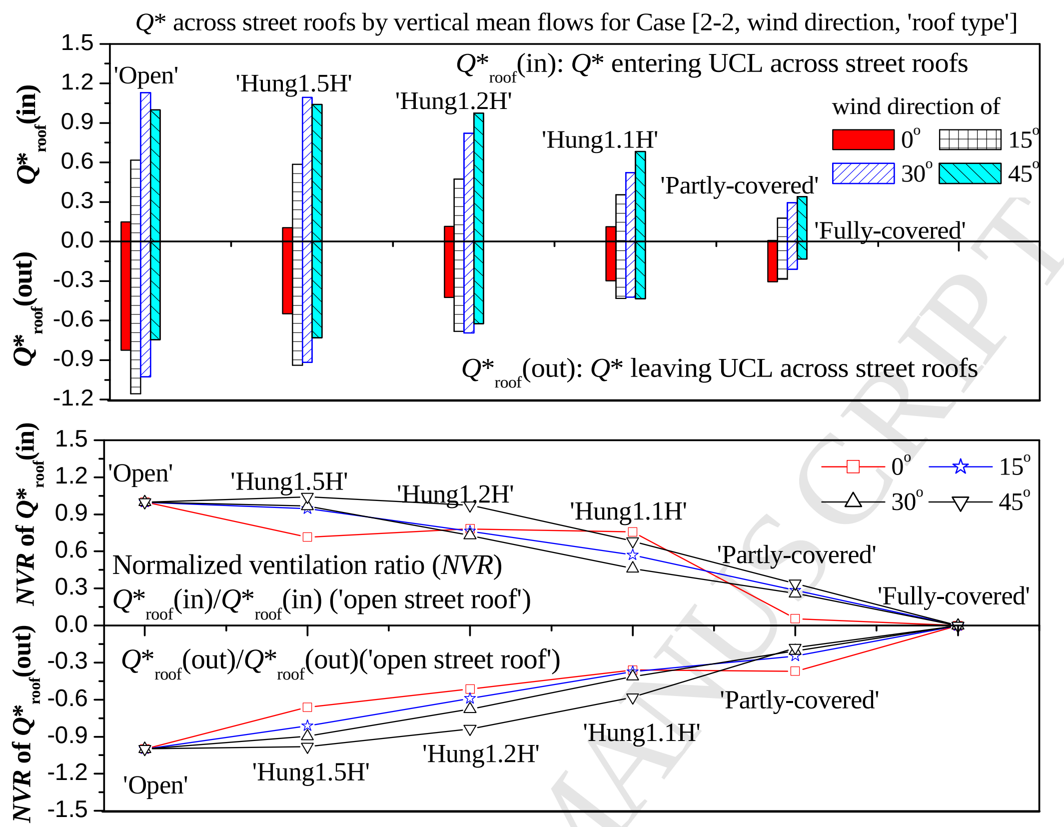

Q* across street roofs by vertical mean flows for Case [2-2, wind direction, 'roof type']
Q*roof(in): Q* entering UCL across street roofs
Q*roof(out): Q* leaving UCL across street roofs
wind direction of
0°
15°
30°
45°
'Open'
'Hung1.5H'
'Hung1.2H'
'Hung1.1H'
'Partly-covered'
'Fully-covered'
Q*roof(in)
Q*roof(out)
Normalized ventilation ratio (NVR)
Q*roof(in)/Q*roof(in) ('open street roof')
Q*roof(out)/Q*roof(out)('open street roof')
NVR of Q*roof(in)
NVR of Q*roof(out)

(a)

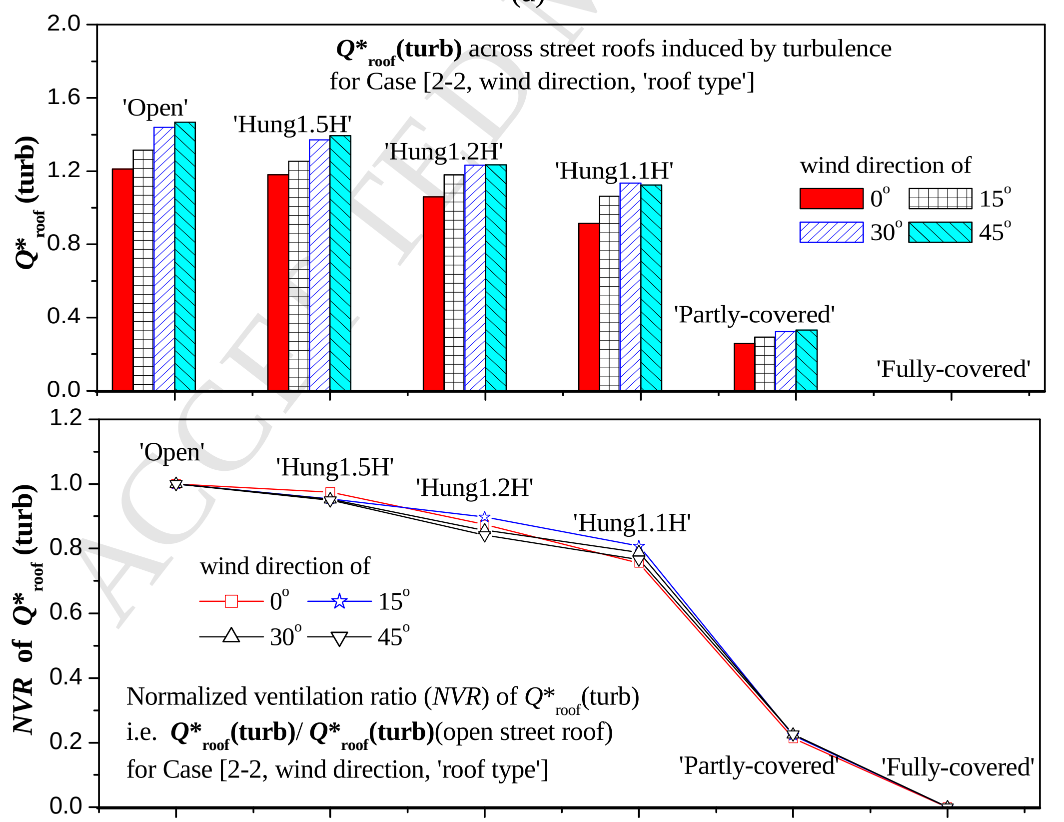

Q*roof(turb) across street roofs induced by turbulence
for Case [2-2, wind direction, 'roof type']
wind direction of
0°
15°
30°
45°
'Open'
'Hung1.5H'
'Hung1.2H'
'Hung1.1H'
'Partly-covered'
'Fully-covered'
Q*roof(turb)
NVR of Q*roof(turb)
Normalized ventilation ratio (NVR) of Q*roof(turb)
i.e. Q*roof(turb)/ Q*roof(turb)(open street roof)
for Case [2-2, wind direction, 'roof type']

(b)

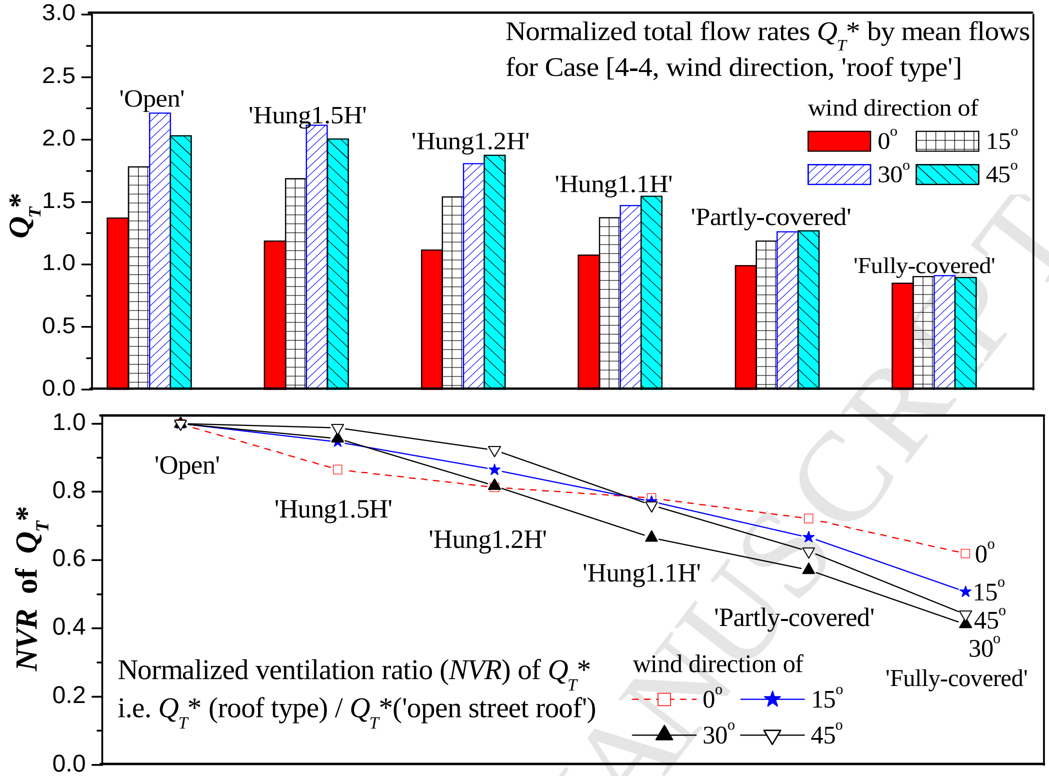

Normalized total flow rates Q_T* by mean flows
for Case [4-4, wind direction, 'roof type']
wind direction of
0° 15° 30° 45°
'Open'
'Hung1.5H'
'Hung1.2H'
'Hung1.1H'
'Partly-covered'
'Fully-covered'
Q_T*
NVR of Q_T*
Normalized ventilation ratio (NVR) of Q_T*
i.e. Q_T* (roof type) / Q_T*('open street roof')

(c)

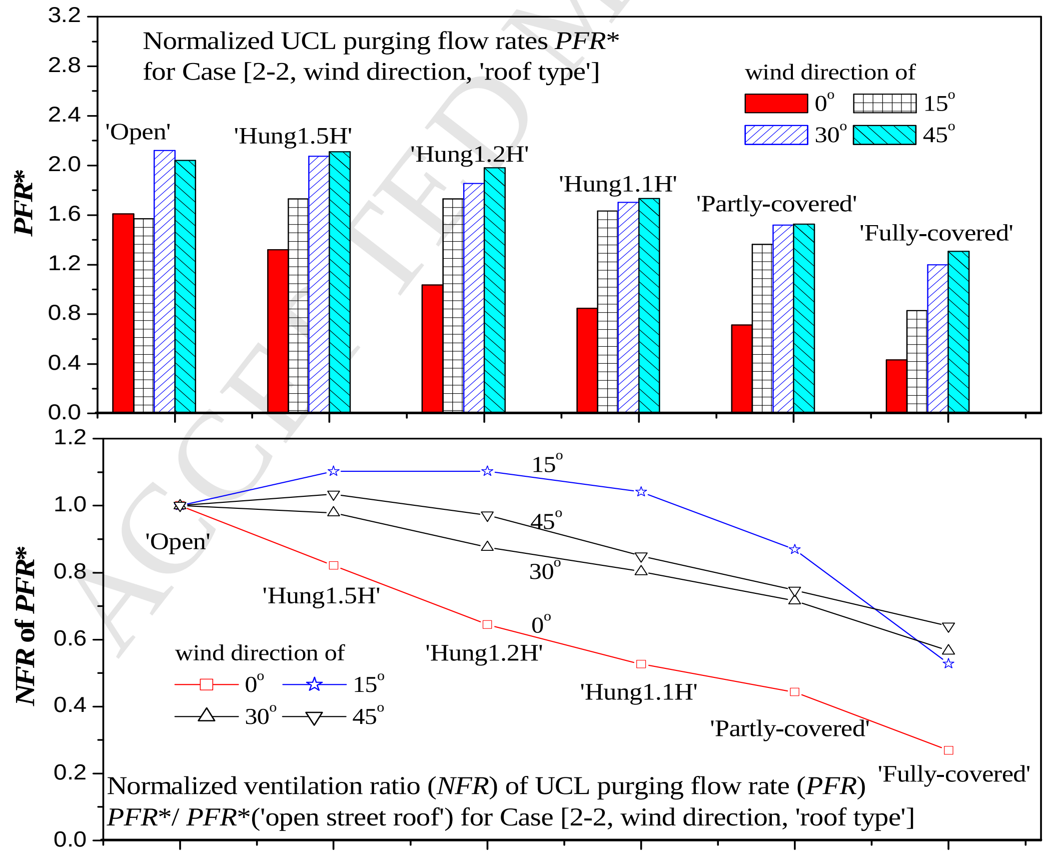

Normalized UCL purging flow rates PFR*
for Case [2-2, wind direction, 'roof type']
wind direction of
0° 15° 30° 45°
'Open'
'Hung1.5H'
'Hung1.2H'
'Hung1.1H'
'Partly-covered'
'Fully-covered'
PFR*
NFR of PFR*
Normalized ventilation ratio (NFR) of UCL purging flow rate (PFR)
PFR*/ PFR*('open street roof') for Case [2-2, wind direction, 'roof type']

(d)

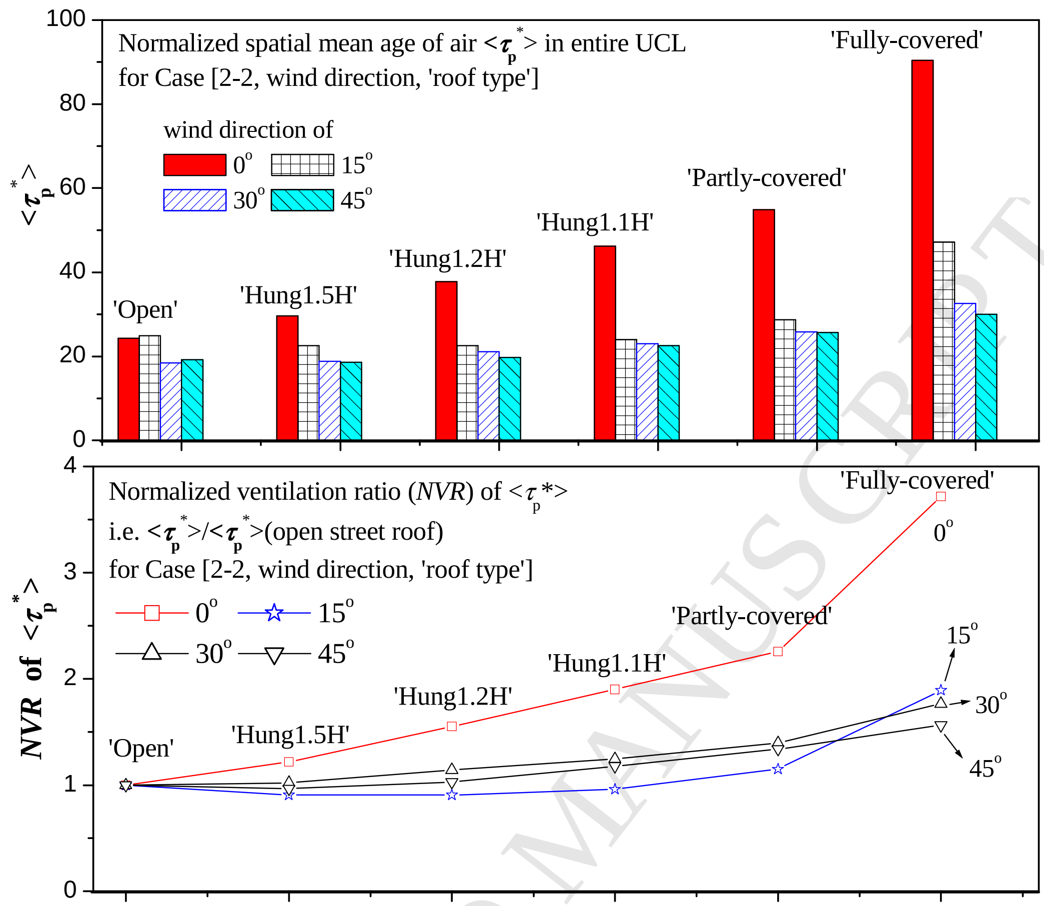

(e)

Fig. 11. Hang et al.

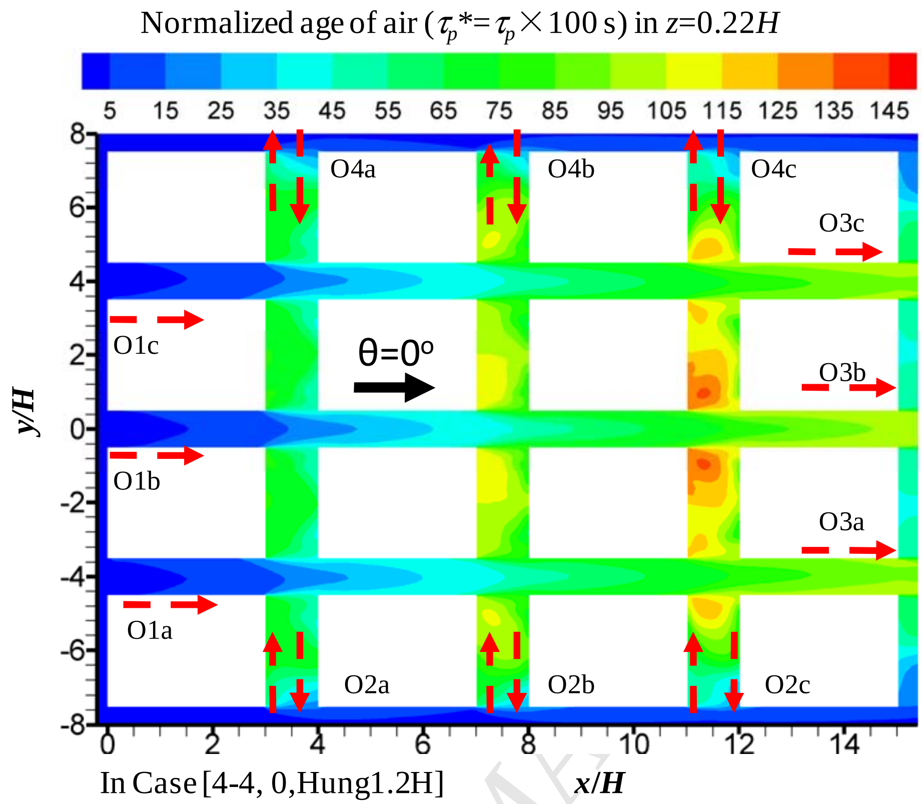
Normalized age of air (τp*=τp×100 s) in z=0.22H
5 15 25 35 45 55 65 75 85 95 105 115 125 135 145
O4a
O4b
O4c
O3c
O1c
θ=0°
O3b
O1b
O3a
O1a
O2a
O2b
O2c
y/H
x/H
In Case [4-4, 0,Hung1.2H]

(a)

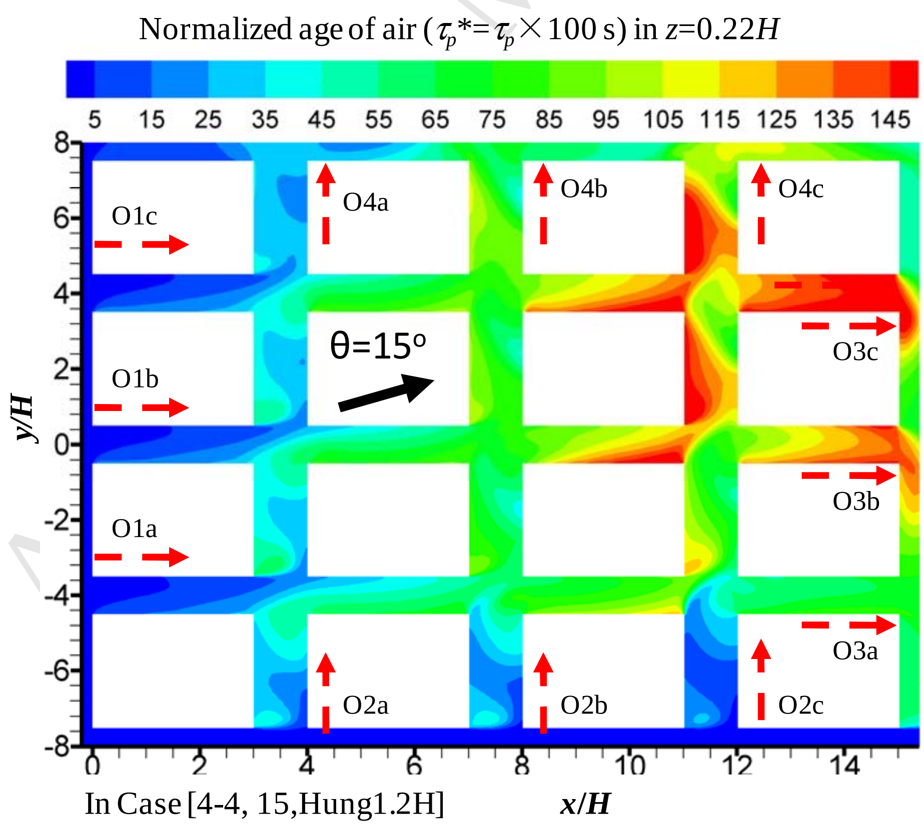
Normalized age of air (τp*=τp×100 s) in z=0.22H
5 15 25 35 45 55 65 75 85 95 105 115 125 135 145
O1c
O4a
O4b
O4c
O1b
θ=15°
O3c
O1a
O3b
O3a
O2a
O2b
O2c
y/H
x/H
In Case [4-4, 15,Hung1.2H]

(b)

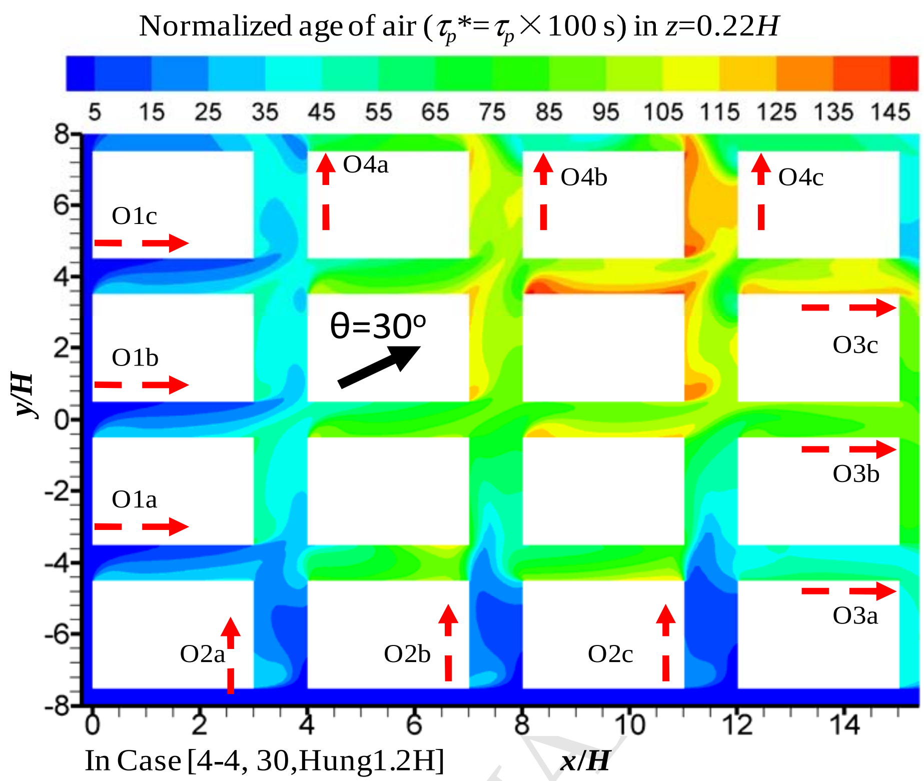

(c)

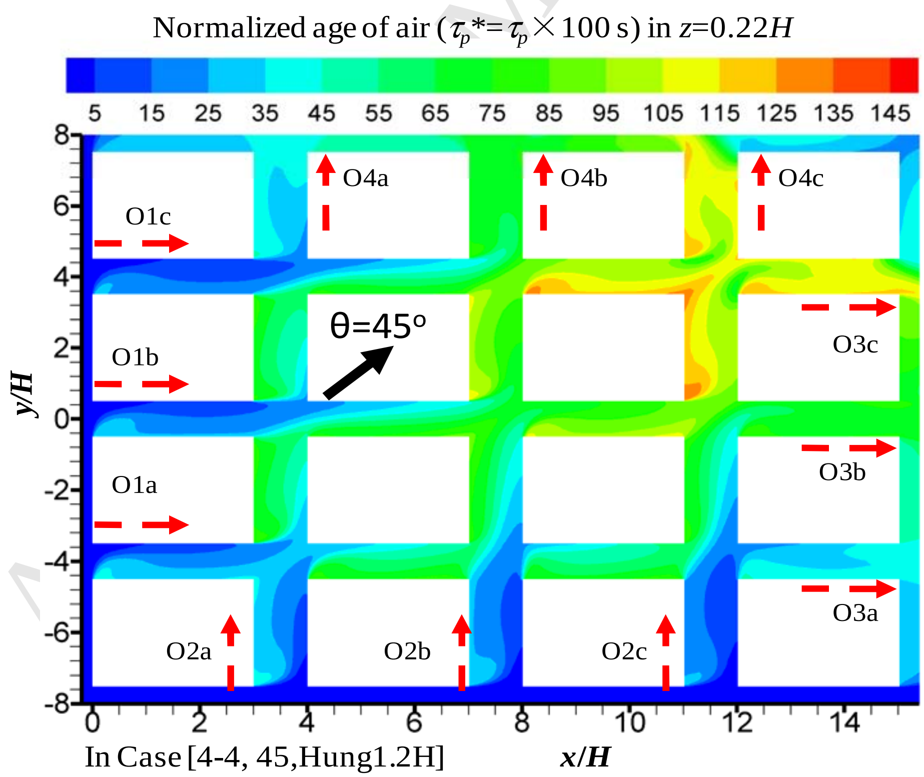

(d)

Fig. 12. Hang et al.

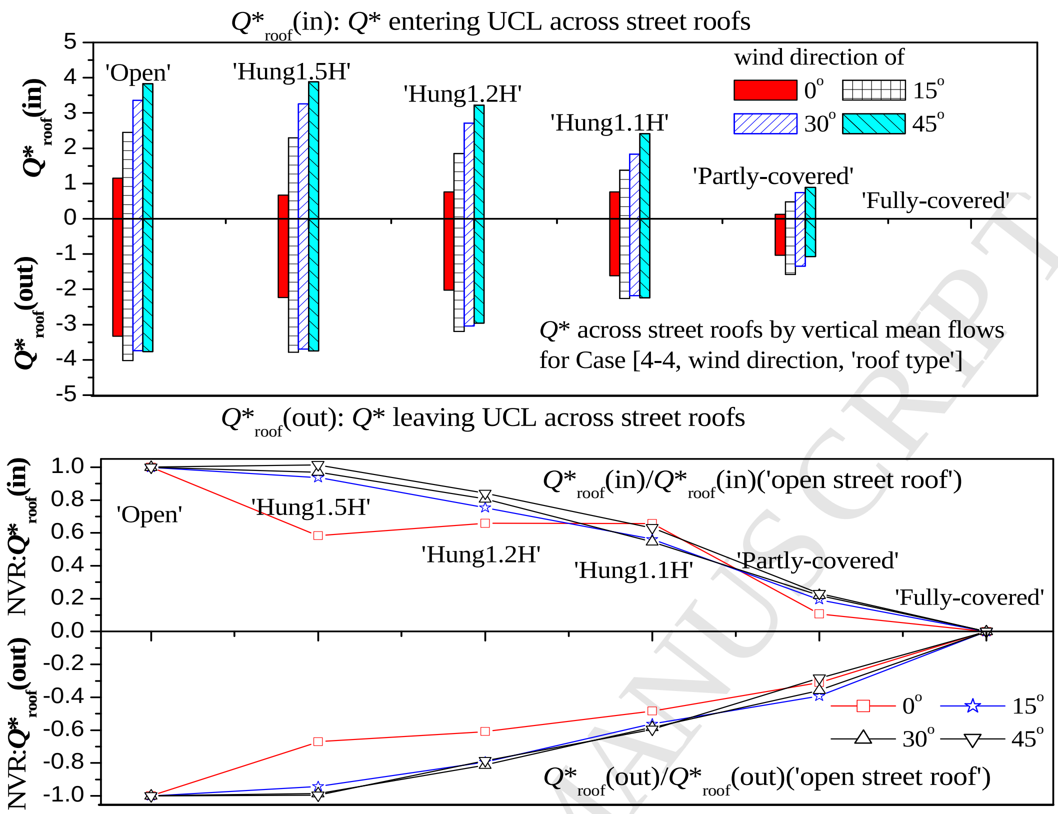

Q*roof(in): Q* entering UCL across street roofs
'Open'
'Hung1.5H'
'Hung1.2H'
'Hung1.1H'
'Partly-covered'
'Fully-covered'
wind direction of
0°
15°
30°
45°
Q*roof(in)
Q*roof(out)
Q* across street roofs by vertical mean flows
for Case [4-4, wind direction, 'roof type']
Q*roof(out): Q* leaving UCL across street roofs
NVR:Q*roof(in)
NVR:Q*roof(out)
Q*roof(in)/Q*roof(in)('open street roof')
Q*roof(out)/Q*roof(out)('open street roof')

(a)

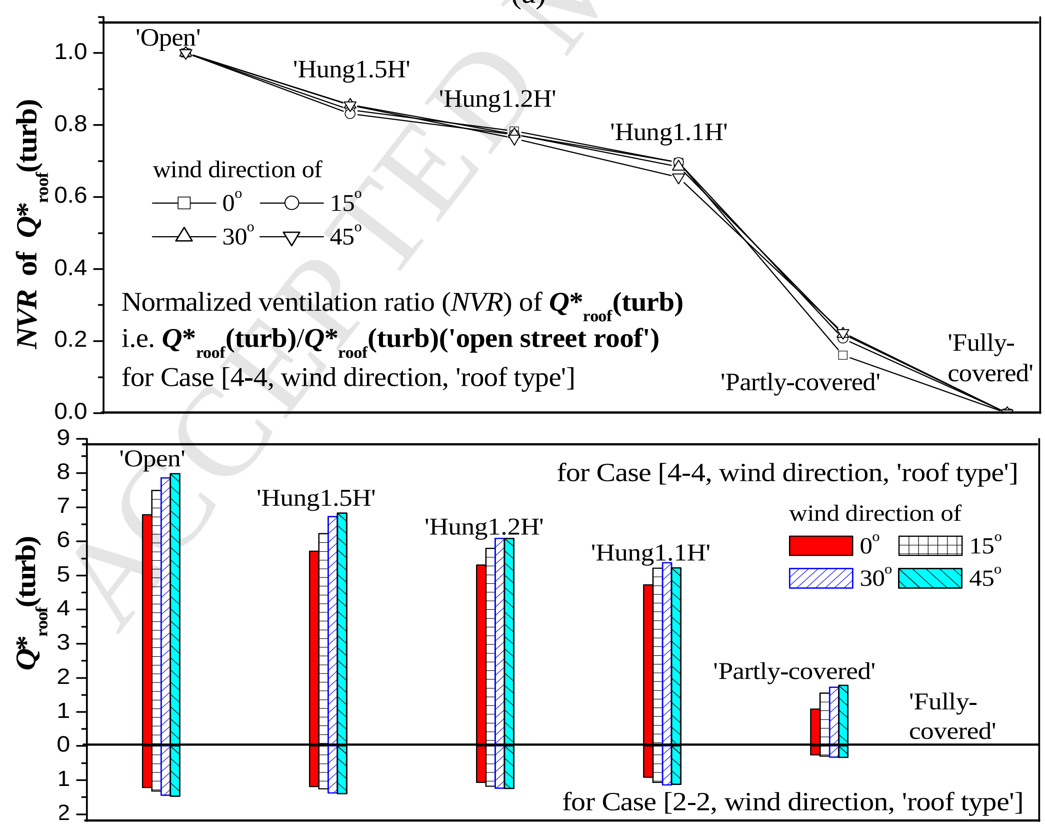

'Open'
'Hung1.5H'
'Hung1.2H'
'Hung1.1H'
'Partly-covered'
'Fully-covered'
wind direction of
0°
15°
30°
45°
NVR of Q*roof(turb)
Normalized ventilation ratio (NVR) of Q*roof(turb)
i.e. Q*roof(turb)/Q*roof(turb)('open street roof')
for Case [4-4, wind direction, 'roof type']
Q*roof(turb)
for Case [2-2, wind direction, 'roof type']

(b)

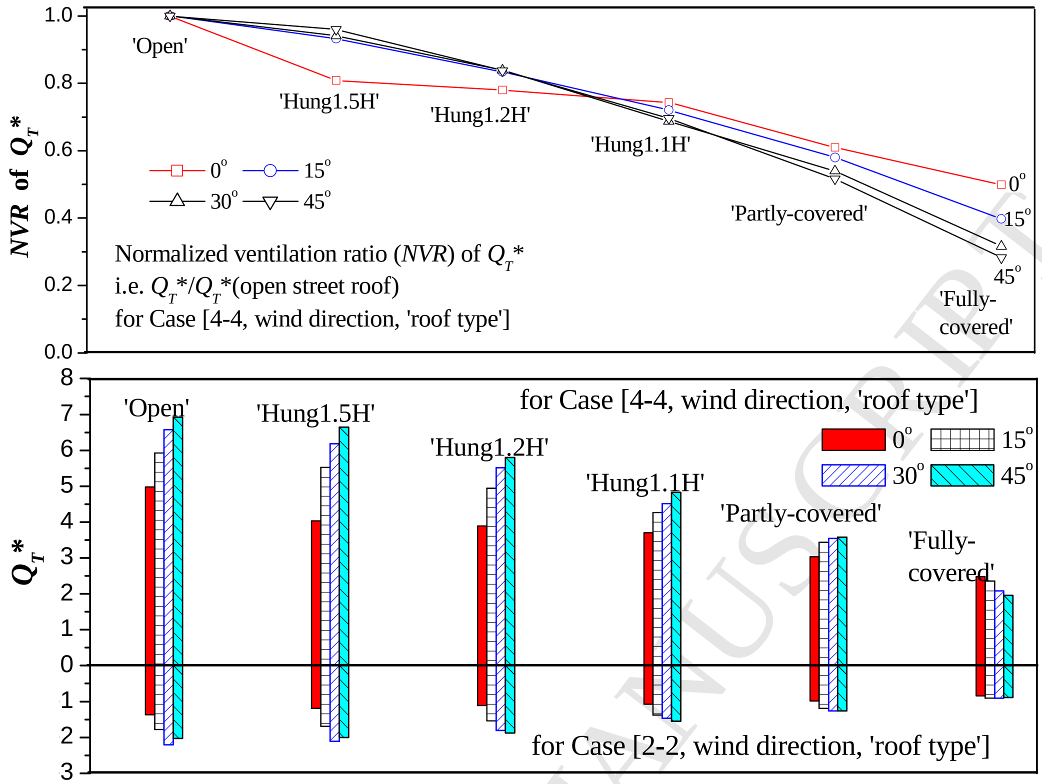

NVR of Q_T*
Q_T*
'Open'
'Hung1.5H'
'Hung1.2H'
'Hung1.1H'
'Partly-covered'
'Fully-covered'
0° 15° 30° 45°
Normalized ventilation ratio (NVR) of Q_T*
i.e. Q_T*/Q_T*(open street roof)
for Case [4-4, wind direction, 'roof type']
for Case [2-2, wind direction, 'roof type']

(c)

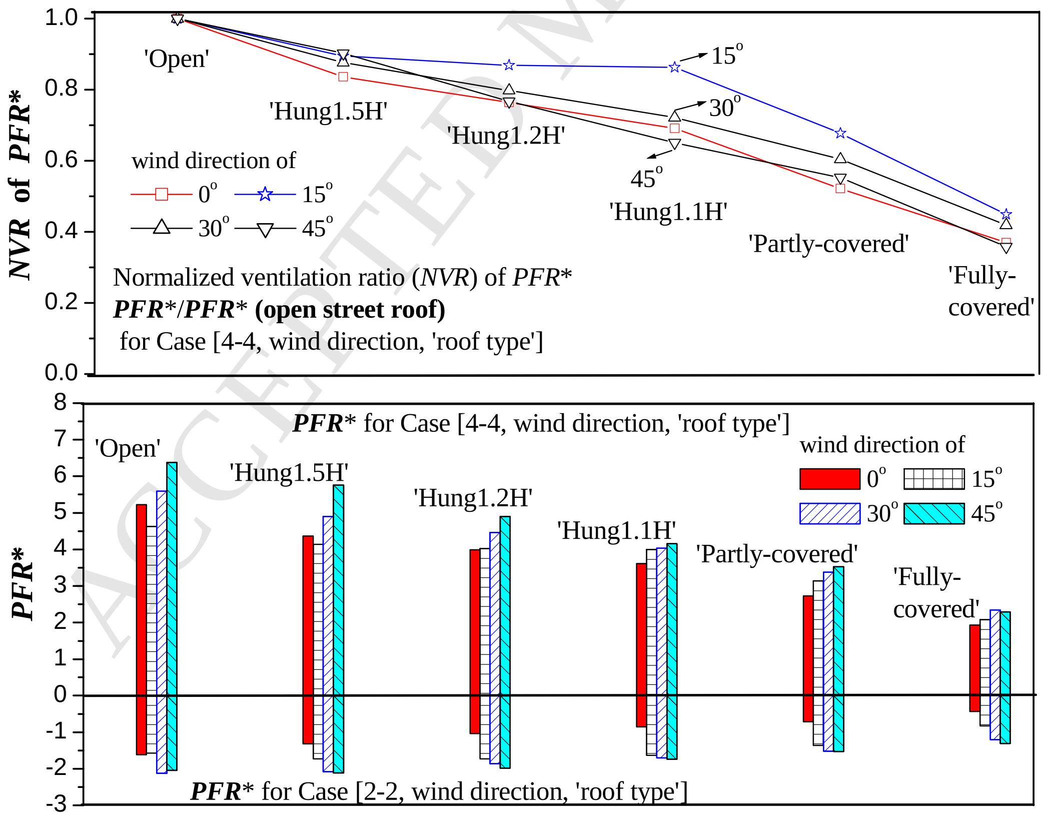

NVR of PFR*
PFR*
'Open'
'Hung1.5H'
'Hung1.2H'
'Hung1.1H'
'Partly-covered'
'Fully-covered'
wind direction of
0° 15° 30° 45°
Normalized ventilation ratio (NVR) of PFR*
PFR*/PFR* (open street roof)
for Case [4-4, wind direction, 'roof type']
PFR* for Case [4-4, wind direction, 'roof type']
PFR* for Case [2-2, wind direction, 'roof type']

(d)

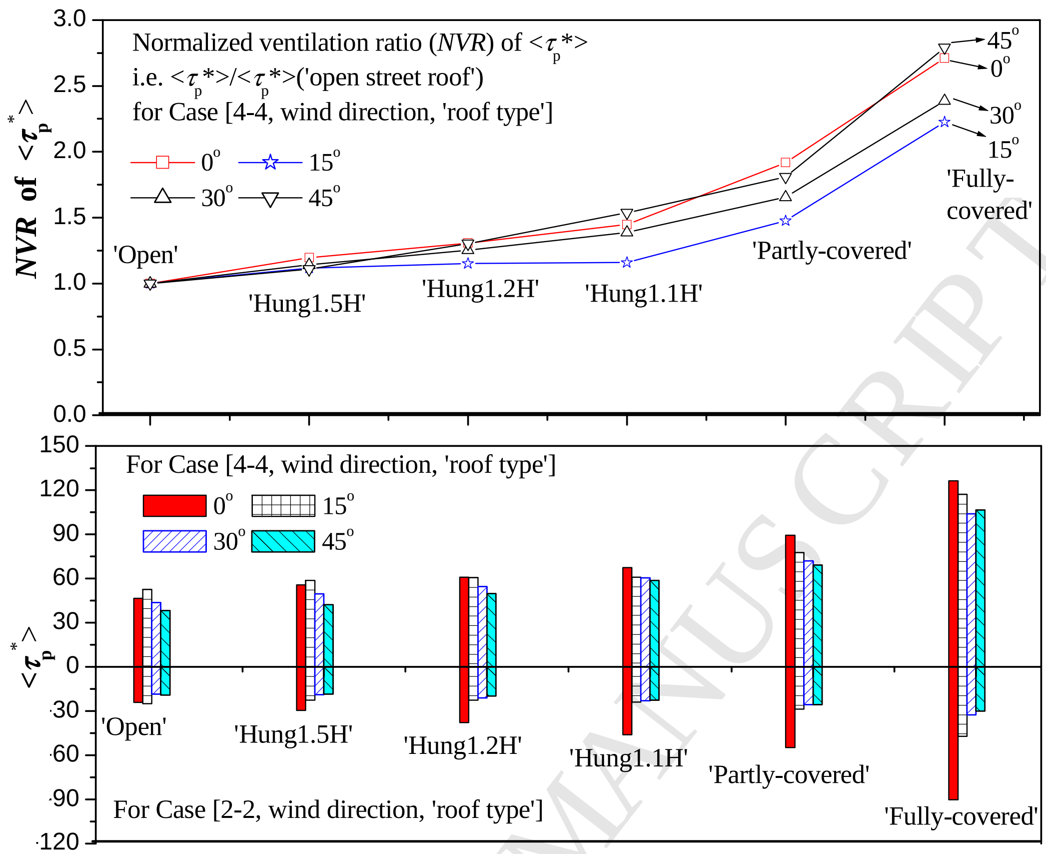

(e)

Fig. 13 Hang et al.

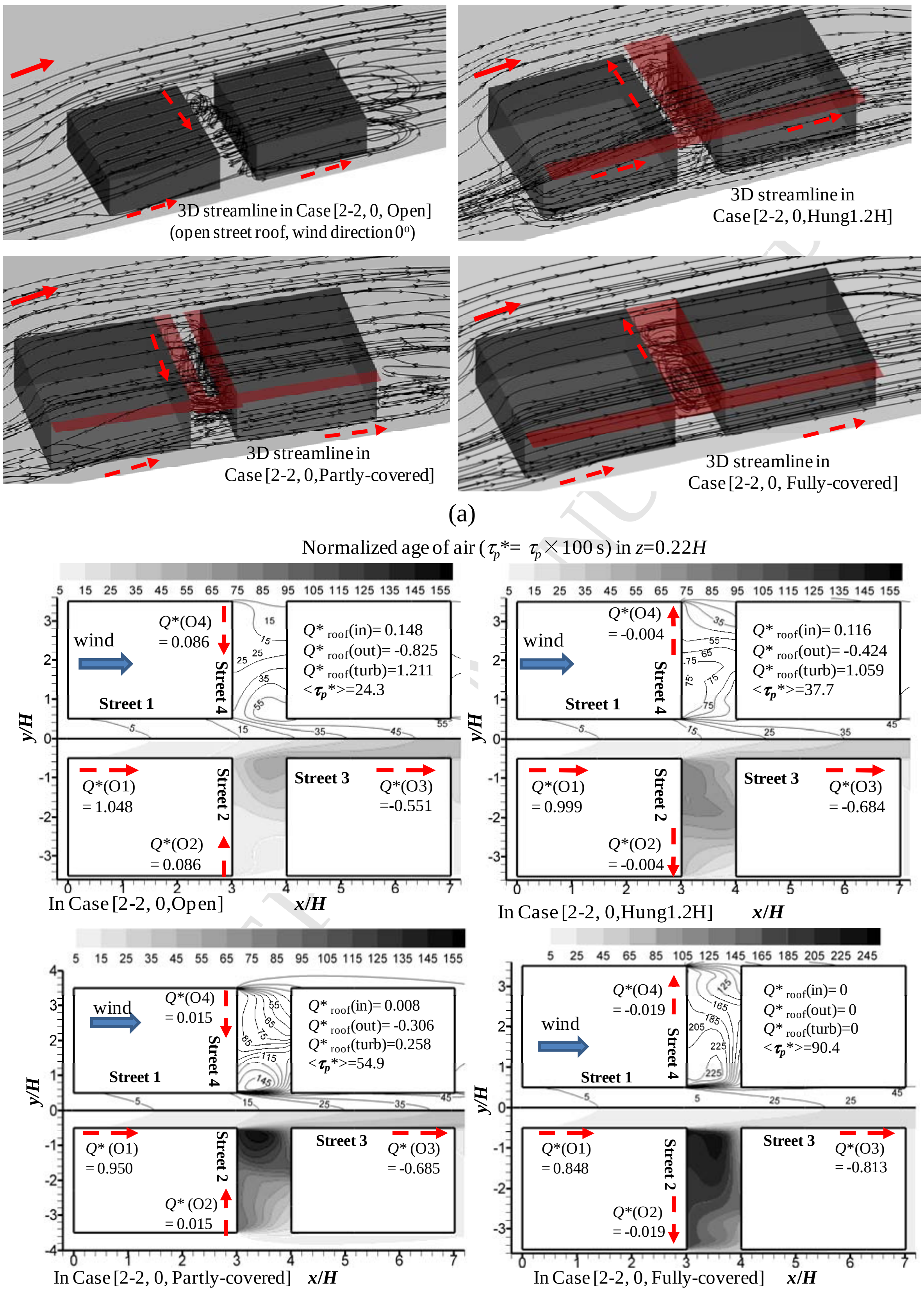

Fig. 6 Hang et al.

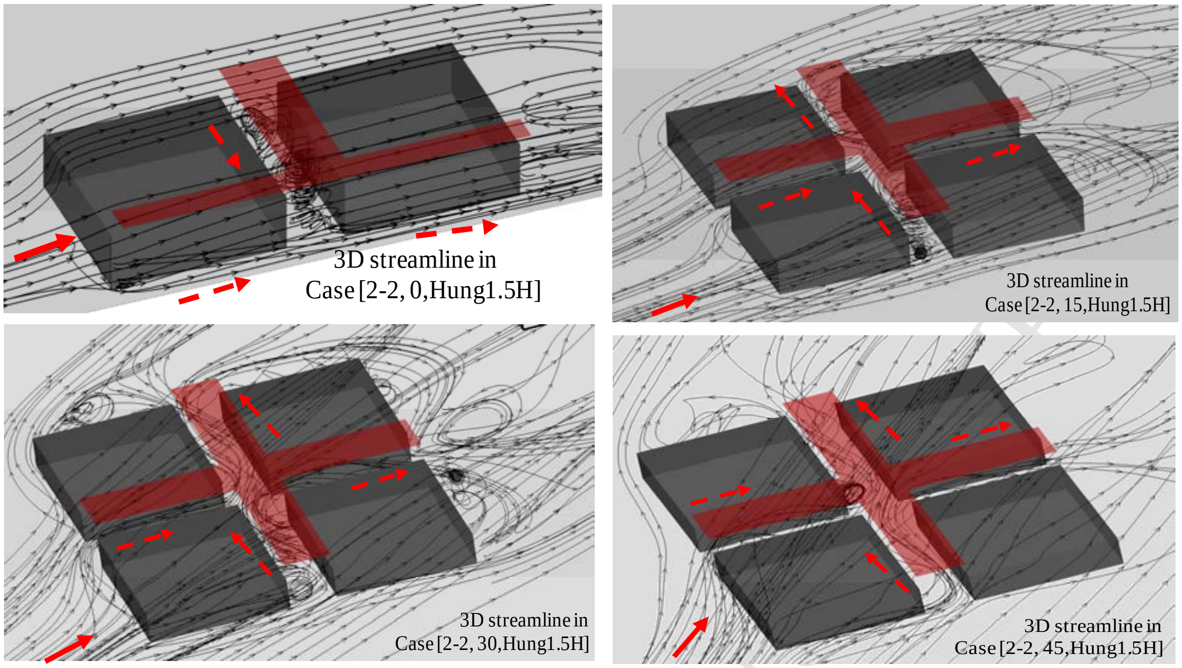

(a)

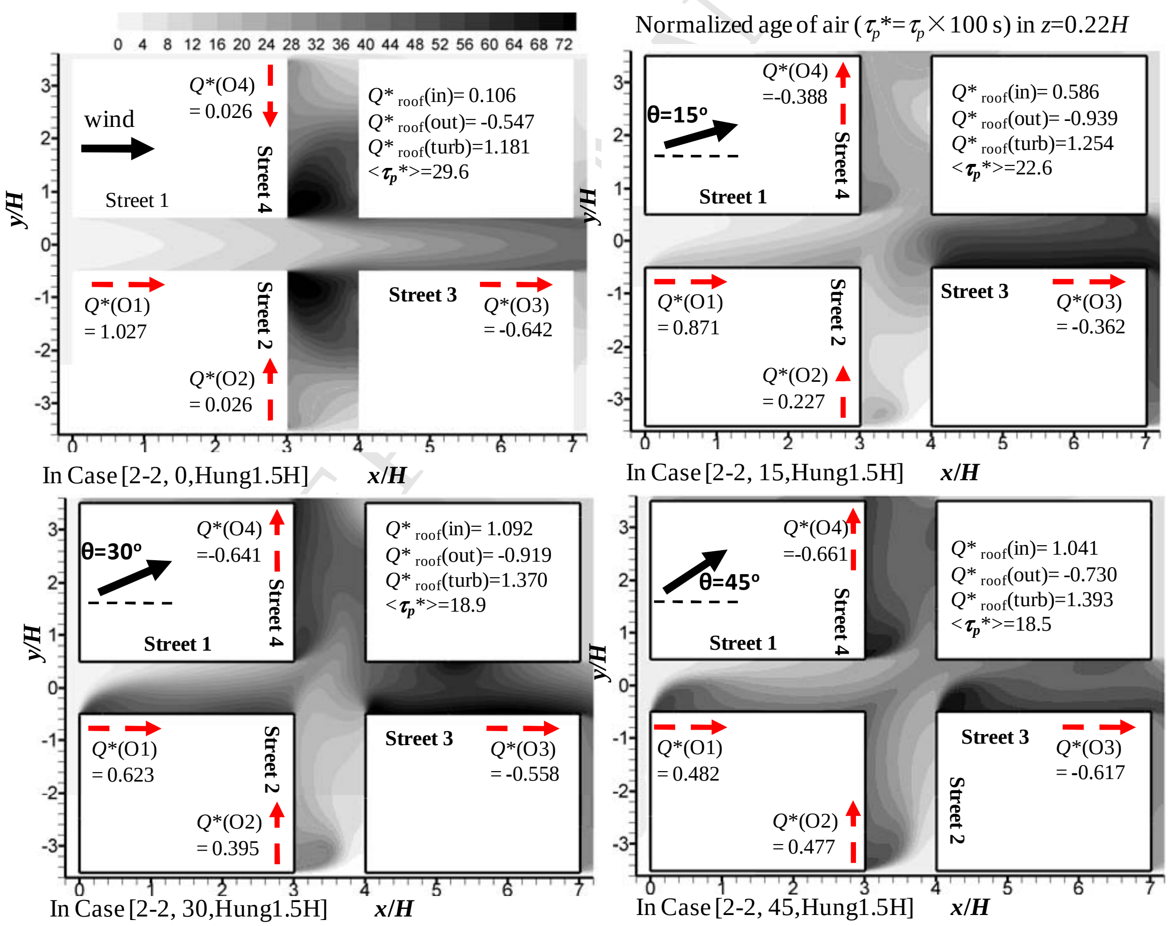

(b)

Fig. 7 Hang et al.

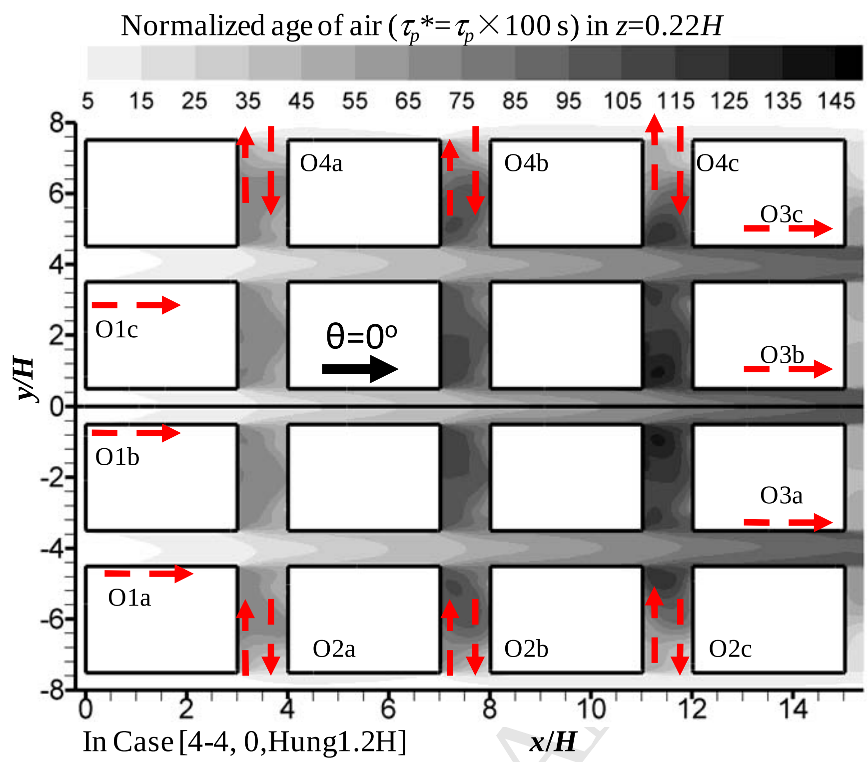
Normalized age of air (τ_p*=τ_p×100 s) in z=0.22H
5 15 25 35 45 55 65 75 85 95 105 115 125 135 145
O4a
O4b
O4c
O3c
O1c
θ=0º
O3b
O1b
O3a
O1a
O2a
O2b
O2c
y/H
x/H
In Case [4-4, 0,Hung1.2H]

(a)

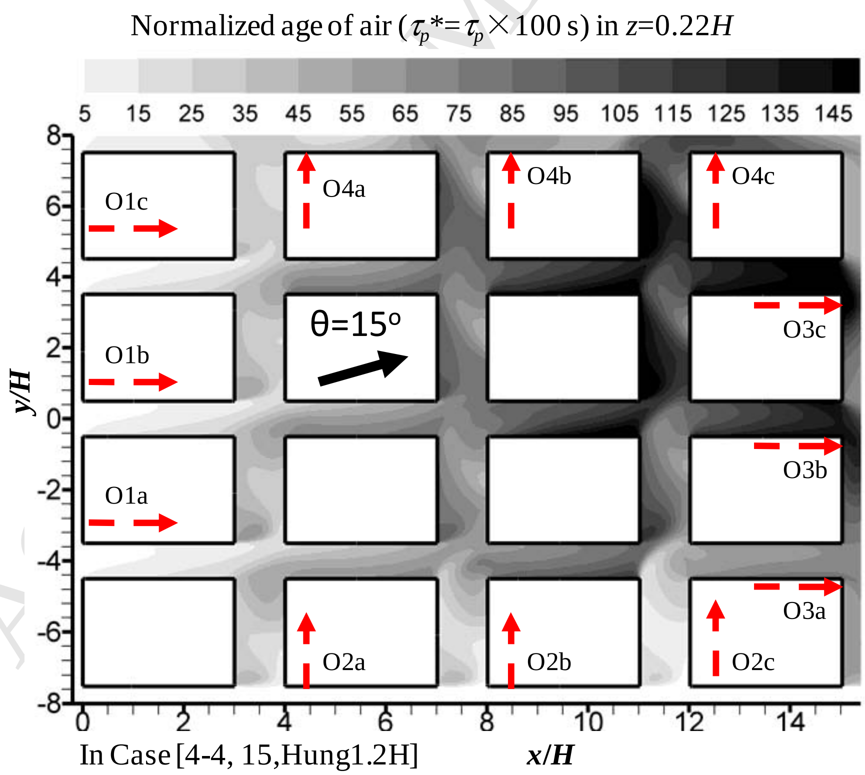
Normalized age of air (τ_p*=τ_p×100 s) in z=0.22H
5 15 25 35 45 55 65 75 85 95 105 115 125 135 145
O1c
O4a
O4b
O4c
θ=15º
O1b
O3c
O1a
O3b
O3a
O2a
O2b
O2c
y/H
x/H
In Case [4-4, 15,Hung1.2H]

(b)

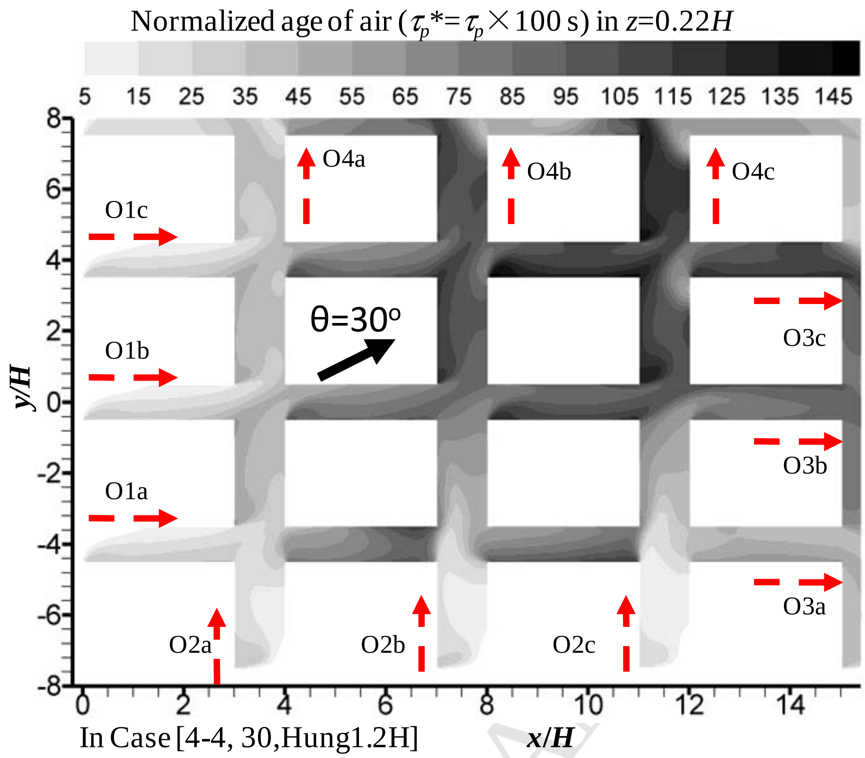

(c)

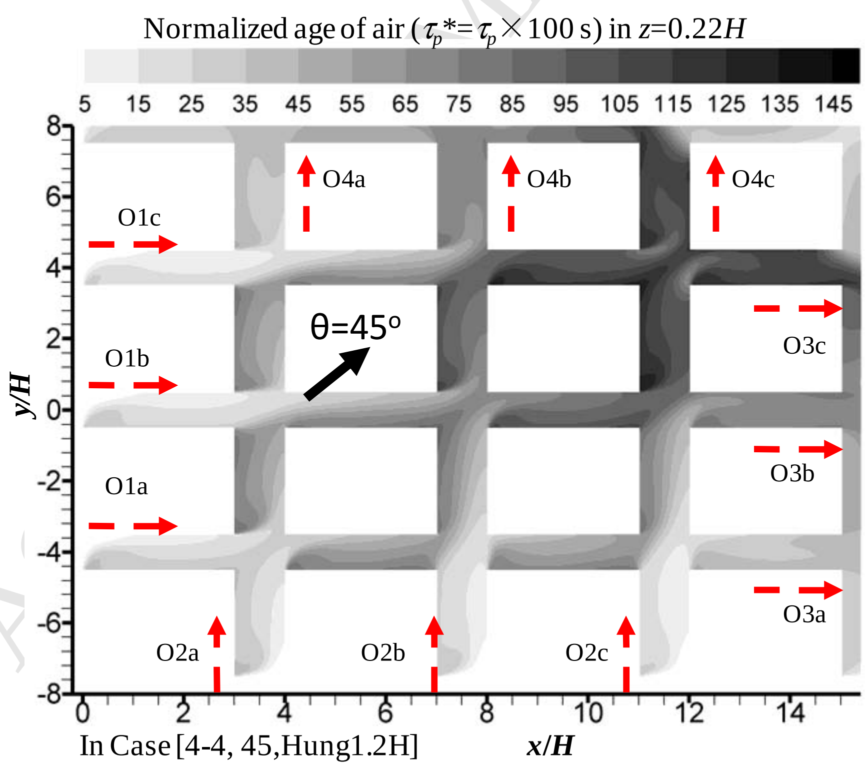

(d)

Fig. 10. Hang et al.